REPUBLIQUE ALGERIENNE DEMOCRATIQUE ET POPULAIRE
MINISTERE DE L'ENSEIGNEMENT SUPERIEUR ET DE LA RECHERCHE SCIENTIFIQUE

UNIVERSITE FERHAT ABBAS - SETIF 1

THESE
Présentée à la Faculté des Sciences
Département de Physique

Pour l'obtention du diplôme de

DOCTORAT ES SCIENCES

Option : Energétique et Mécanique des Fluides

Par

BENSALEM Salaheddine

THEME

Contribution to the study of physical properties of CZTX (X=S, Se) solar materials

Soutenue le : 22/01/2015

Devant le jury composé de :

Président :	Dr ALI SAHRAOUI Ferhat	Prof.	U. Ferhat Abbas - SETIF 1
Rapporteur :	Dr CHEGAAR Mohamed	Prof.	U. Ferhat Abbas - SETIF 1
Examinateur :	Dr HADJ ARAB Amar	DR	CDER - Alger
Examinateur :	Dr CHARIFI Zoulikha	Prof.	U. Mohamed Boudiaf - M'sila

بسم الله الرحمن الرحيم

Acknowledgement

I would like to acknowledge and send sincere thanks to my superb advisor Dr. **CHEGAAR Mohamed** Professor at Setif-1 University for his guidance and patience during my graduate and post-graduate study and also during my research activities.

I would like to thank my thesis committee members:
Dr. **ALI SAHRAOUI Ferhat** Professor at Setif-1 University who honored our work by accepting the chairmanship of the committee.

My deep gratitude to Dr. **HADJ ARAB Amar** Director of Research at the Center for Development of Renewable Energies and Dr. **CHARIFI Zoulikha** Professor at M'sila University; whose agreed to examine the thesis.

I would like to acknowledge my parents and my family.

Finally, my sincere thanks to all those who have contributed from near or from far to accomplish this work.

CONTENTS

Chapter 1: Solar Materials for Photovoltaic Conversion

Chapter 2: Theoretical Study of Fundamental Properties of CZTX (X=S and Se)

Chapter 3: Results and Discussion

Appendix

LIST OF FIGURES

CHAPTER 1

CHAPTER 2

CHAPTER 3

APPENDIX

LIST OF TABLES

CHAPTER 1

CHAPTER 2

CHAPTER 3

Introduction

INTRODUCTION

Preamble

Photovoltaic solar energy is expected to be one of the most important renewable energies resources for energy challenges. The widespread use of solar cells as device for photovoltaic applications requires the development of absorber layers for solar cells, which should take into account the cost, and the cleanly of alloys for a suitable development.

Some solar materials have particular physical properties, which are sources of fundamental and technological interest. In solar photovoltaic applications, silicon; is the most prominent and most studied semiconductor. However, the efficiency of solar cells based on silicon remains limited with a high production cost. For this, in the recent years research activities focus on the investigation of new solar materials to improve energy efficiency and lower cost of production taking into account the environmental aspect.

The I_2-II-IV-VI_4 (I=Cu, Ag; II=Zn, Cd; IV=Si, Ge, Sn; VI=S, Se) series of quaternary chalcogenide semiconductors are solar materials that have drawn wide interest for their potential application as solar-cell absorbers, photocatalysts for solar water splitting and thermoelectric materials. For example, Cu_2ZnSnS_4 (CZTS) and $Cu_2ZnSnSe_4$ (CZTSe) are naturally abundant and environmental friendly solar materials for thin-film solar-cell absorbers, which have shown conversion efficiencies as high as 10 % [1].

Problematic, motivation and main aims of this thesis

The quaternary semiconductors Copper-Zinc-Tin-(Sulphide, Selenide) Cu_2ZnSnX_4 (X=S and Se) abbreviated CZTX (X=S and Se) are veritable candidate solar materials as absorber layers for thin films based solar cells, and that for several considerations; all constituents of this quaternary alloys are abundant on the earth's crust and are not toxic, optimal direct band gap of about 1.5 eV and high absorption coefficient (above of 10^4 cm^{-1}) [2, 3], furthermore, CZTSSe based solar cells have low temperature coefficients [4, 5].

In the literature, several theoretical works discussed the fundamental properties of CZTX [6, 7, 8]. Most theoretical works on CZTX[1] compounds considered mainly electronic and optical properties. Despite much earlier effort, our understanding of fundamentals properties especially mechanical and thermodynamic properties and their behavior under external disturbance pressure and temperature is still far from satisfactory.

---

[1] In this manuscript for CZTX; X means S and Se.

From structural viewpoint, for CZTX compounds, three types of crystal structure have been reported: kesterite (KS), stannite (ST) and wurtz-stannite type (WZ-stannite) [9]. Because of that energy difference between KS (space group $I\bar{4}$) and ST type (space group $I\bar{4}2m$) is small (few meV/atom) [6, 8] both structures can coexist in synthesized samples. In fact, a comparative investigation of the physical properties of both types for both alloys is very significant; in other words, necessary.

Therefore, the aim of this work is to provide further information concerning mainly the elastic and thermodynamic properties of CZTX as novel solar material absorbers for the KS and ST types, and then to take advantage of the properties of CZTX for thin films based solar cells, for eventual photovoltaic technological applications.

Structure of this manuscript

This manuscript consists of three chapters. In the first chapter, we present some arguments concerning the need of renewable energy, and then we deal with some solar materials for solar energy applications and we focus on the new alloys CZTX as attractive solar materials for photovoltaic application.

The second chapter deals with theoretical study of fundamental properties of CZTX solar materials, we summarize previous theoretical works on these compounds. Then, we present our contribution to investigate physical properties of these alloys and the method of calculation used in this work.

In the third chapter, we present our foremost obtained results, such as, structural properties (lattice parameters, bulk modulus and its derivative), the elastic properties (elastic constants, moduli of elasticity, the propagation velocities of the elastic waves and Debye temperature), the effect of a hydrostatic pressure on those parameters is also studied. Thermodynamic properties (thermodynamic functions and heat capacity) for CZTX compounds respectively, in the KS (space group $I\bar{4}$) and ST type (space group $I\bar{4}2m$) structure are also presented.

Finally, we conclude our work by a general conclusion, which includes the main theoretical results obtained through this study.

The theoretical framework of the calculation tool is the subject of the thesis-appendix entitled "Density Functional Theory: Major Tool in Computational Materials Science"; where we explain the Derivation and formalism of the Density Functional Theory.

References

[1] S. Chen, A. Walsh, Y. Luo, J. H. Yang, X. G. Gong, S. H. Wei, Physical review B 82 (2010) 195203.

[2] N. Nakayama, K. Ito, Appl. Surf. Sci. 92 (1996) 171.

[3] S. Chen, X. G. Gong, A. Walsh, S. H. Wei, Appl. Phys. Lett. 96 (2010) 021902.

[4] J. Krustok, R. Josepson, M. Danilson, D. Meissner, Solar Energy 84 (2010) 379.

[5] S. Bensalem, M. Chegaar, M. Aillerie, Energy Procedia, 36 (2013) 1249.

[6] S. Chen, X. G. Gong, A. Walsh, S. H. Wei, Appl. Phys. Lett. 94 (2009) 041903.

[7] C. Persson, J. Appl. Phys. 107 (2010) 053710.

[8] S. Botti, D. Kammerlander, M. A. L. Marques, Appl. Phys. Lett. 98 (2011) 241915.

[9] X. He, H. Shen, Physica B 406 (2011) 4604.

Chapter I

Solar Materials for Photovoltaic Conversion

I.1. Preamble

In this introductory chapter, we expose some arguments concerning the need of renewable energy; because of the increasing demand for energy, climate change and environmental impacts of fossil energy exploitation. Then we focus on the photovoltaic application as an important alternative resource for future-energy challenges. We talk about some solar materials for solar energy applications. We cite the main technologies, such as, silicon based solar cells, cadmium tellurium (CdTe) and copper (indium, gallium) selenium (CIGS) based thin films solar cells, and we focus on the new alloys CZTX as attractive solar materials for solar photovoltaic energy conversion.

I.2. Need of renewable energy

The world rapidly increasing demand for energy beyond 13 TW/year accelerates fossil fuel consumption associated with CO_2 emissions and global warming issues [1]. Renewable energy is a carbon free and sustainable energy sources. It becomes the optimal approach to face climate change problems.

Renewable energy sources, such as hydroelectricity, wind, and solar power, are important for the production of electricity to address the needs of a growing population without destroying the environment. Renewable energy can replace conventional fuels in four distinct areas: electricity generation, hot water and space heating, motor fuels, and rural (off-grid) energy services. We talk about some renewable energy types to highlight the authenticity of these resources; we focus on the hydroelectricity energy, wind energy, marine energy, biofuel energy and solar energy.

I.2.1. Hydroelectricity energy

Hydroelectricity is the term referring to the electricity generated through hydropower, or also; the production of electricity using the gravitational force of falling or flowing water. It is considered as the most widely used form of renewable energy, accounting for 16 % of global electricity generation in 2010 [2].

The major advantage of hydroelectricity is the relatively low cost, which makes it a competitive source of renewable electricity. The average cost of electricity from a hydropower station larger than 10 MW is 3 to 5 U.S. cents per KWh [2]. Hydroelectric plants exhibit a long operating life, which can exceed a half of century.

I.2.2. Wind energy

Historically, the first utilization of wind energy was to sail ships in the Nile some 5000 years ago [3]. However, several civilizations used wind power for numerous purposes. The Europeans exploited wind to grind grains and pump water in the 1700s and 1800s [3].

The first windmill to produce electricity was performed in 1890 in the United States. An experimental grid connected turbine with a capacity greater than 2 MW was installed in 1979 on Howard Knob Mountain; North Carolina (USA), a 3 MW turbine was installed in 1988 on Berger Hill in Orkney (Scotland) [3].

Airflows are employed to operate wind turbines. Modern wind turbine for utility-scale power generation range from 600 kW to 5 MW of rate power, nevertheless, turbines with rate output of 1.5-3 MW have become the most routinely installed for commercial scale. The available power from the wind is proportional to the cube of the wind speed [3]; the increasing of wind speed leads to an increasing of the output power up to a maximum power. Areas where winds are stronger and more stable, such as offshore (Fig1.1) and high altitude sites are favorite locations for wind farms.

Recently, several factors have contributed to the declining of large-scale wind energy generation costs, such as; improvement of turbine designs and plant utilization. In the United States, the cost of wind-generated electricity decreased from 35 cents per kWh in 1980 to around 4 cents per kWh in 2004 at favorable locations [3] (Fig1.2). It is noted that, with this price; wind energy has become the least costly new source of electric power, *i.e.* less costly than nuclear, coal, oil, and natural gas [3].

Fig.1.1: *Wind energy offshore farm* [3].

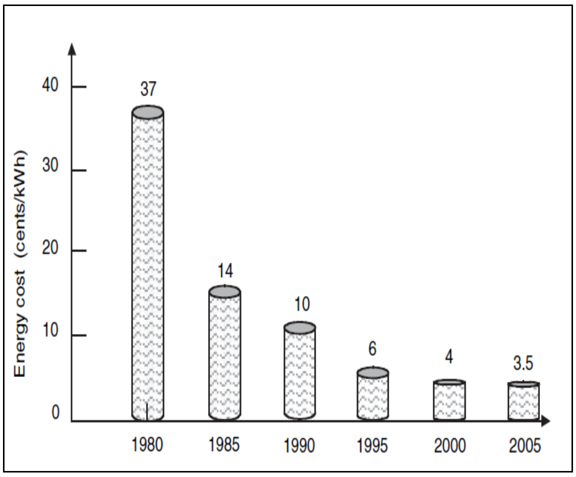

Fig.1.2: *Declining cost of wind-generated electricity in USA* [3].

I.2.3. Marine energy

Marine energy, as well called ocean energy, refers to the energy carried by ocean waves, tides, salinity and ocean temperature differences. The movement of water in the oceans creates a vast store of kinetic energy. This energy; may be harnessed to generate electricity. The conversion of the ocean waves into electricity is performed through a building to the coast, within sealed chamber *i.e.* the capture chamber (Fig1.3). The construction is equipped with turbines, which drive alternators. The turbines work by the compression of the air under the rise and the descent of the waves, consequently; alternators attached to active turbines can produce electricity.

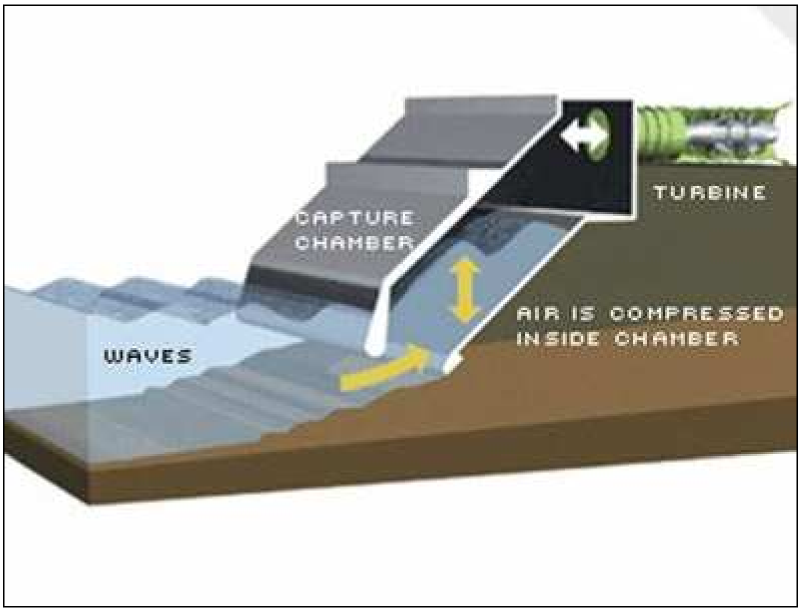

Fig.1.3: *Operating mechanism of wave power station* [4].

The tidal power station, which consists mainly of barrages and turbines, is another marine energy. The first tidal power station in the world is the 240 MW "La Rance" tidal barrage, which began generating power off the French coast in 1966 [5]. Ocean energy saw slight growth for decades, however currently, numerous modern commercial projects are operational, and other projects are in development in several littoral countries.

An estimated 6 MW of ocean energy is operational or being tested in European (off the coasts of Denmark, Italy, the Netherlands, Norway, Spain and the United Kingdom), with additional off-shores projects located principally in Canada, India, Japan, South Korea and United States. Ocean energy has the potential of providing a considerable amount of new renewable energy around the world. Presently, at least 25 countries are involved in ocean energy development and research activities [5].

The quantity of energy carried by waves and tidal streams, which is convertible to electrical power has been evaluated in numerous preceding studies. Building Options[1] for United Kingdom "UK" Renewable-Energy, indicated a practical worldwide wave energy resource within the interval 2000 and 4000 TWh/year, whereas, the UK practical offshore wave energy resource has been evaluated by 50 TWh/year [6].

I.2.4. Biofuel energy

Biofuel is a renewable energy source produced from natural substances [7]. The most widespread biofuels, which can be used as a substitute for petroleum fuels are; ethanol and biodiesel. The ethanol can be produced from corn, wheat or sugar beet, however; the biodiesel can be made from oil seeds.

Production of ethanol from biomass is an important way to decrease the consumption of oil and their adverse impacts on the environment. Likewise, the growing interest in the use of vegetable oils for making biodiesel, which is less polluting than conventional petroleum diesel fuel, may contribute to the protection of the environment.

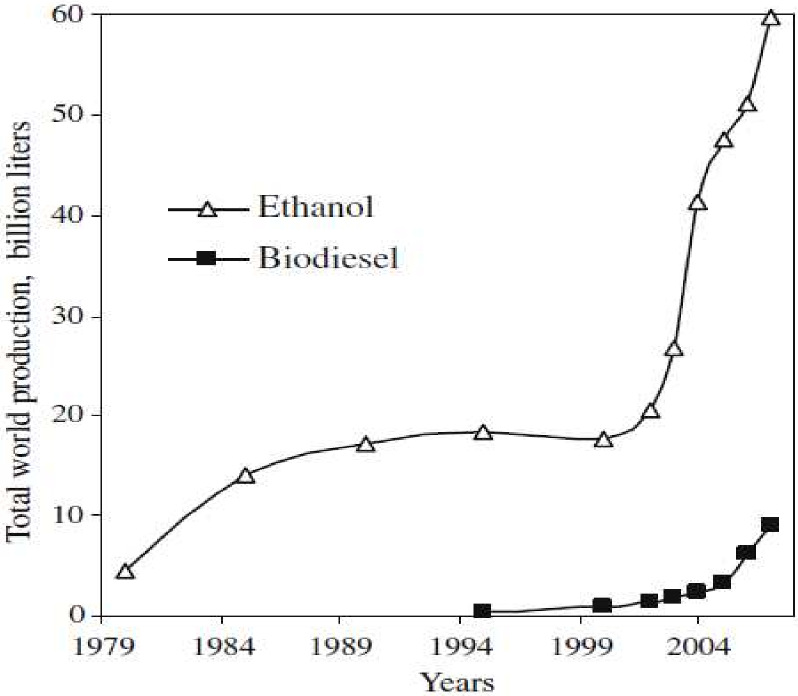

Fig.1.4: *World production of ethanol and biodiesel (1980-2007)* [7].

Biofuels possess several advantages; there are summarized in the following points [7]:

- ✓ Biofuels are effortlessly available from ordinary biomass sources;

---

[1] Building Options Limited is a Chartered Building Consultancy in UK.

- ✓ They represent a carbon dioxide cycle in combustion;
- ✓ They exhibit an enormous ecological potential;
- ✓ Using biofuels leads to various benefits for the environment, economy and consumers;
- ✓ They are biodegradable and contribute to sustainable development.

The world productions of ethanol and biodiesel between 1980 and 2007 are shown in Fig.1.4. The observed increase enhances the authenticity of these renewable resources.

I.2.5. Solar energy

Solar energy, is harnessed using a range of ever-evolving technologies such as; solar photovoltaic, solar heating, solar thermal electricity and solar architecture. Solar technologies; are broadly characterized as either passive solar or active solar depending on the way they capture, convert and distribute the solar energy.

Passive solar techniques; based on a smart solar architecture, in which the respect of some architectural principles allow to passive exploitation of solar radiation energy, include: building orientation, selecting materials with favorable thermal mass or light dispersing properties, and designing spaces that naturally circulate air.

Active solar techniques include the use of photovoltaic panels and solar thermal collectors to convert the energy of solar radiation.

The solar thermal power system collects the thermal energy in solar radiation and uses it at high or low temperatures [3]. Low-temperature applications include heat water preparation and spaces heating. While, high-temperature applications consist to concentrate the sun’s heat energy to produce steam for driving electrical generators.

Concentrating solar power (CSP) technology has the ability to store thermal energy from sunlight and deliver it in the form of electrical energy during dark or high-demand periods. The convenience of the concentrating solar power has been demonstrated on a commercial scale, as a result, CSP technology promises to deliver low-cost, high-value electricity on a large scale. Fig.1.5; is a schematic representation of a large-scale solar thermal power station that serves to the production of electricity.

Solar photovoltaic energy is the conversion of sunlight into electricity directly through photovoltaic effect. Photovoltaic effect consists to convert light into electric current. Photovoltaic is an important and relatively inexpensive source of electrical energy for both variants: grid-connected and isolated sites electric supply. Furthermore, other applications also exist, such as, spatial applications in satellites and solar powered calculators.

The amount of energy from the sunlight, which strikes the earth each hour, is more than the energy that the entire population of the world consumes in a year. Hence, energy from the sun is unlimited, if only it could be converted directly to electricity or fuels at a competitive cost.

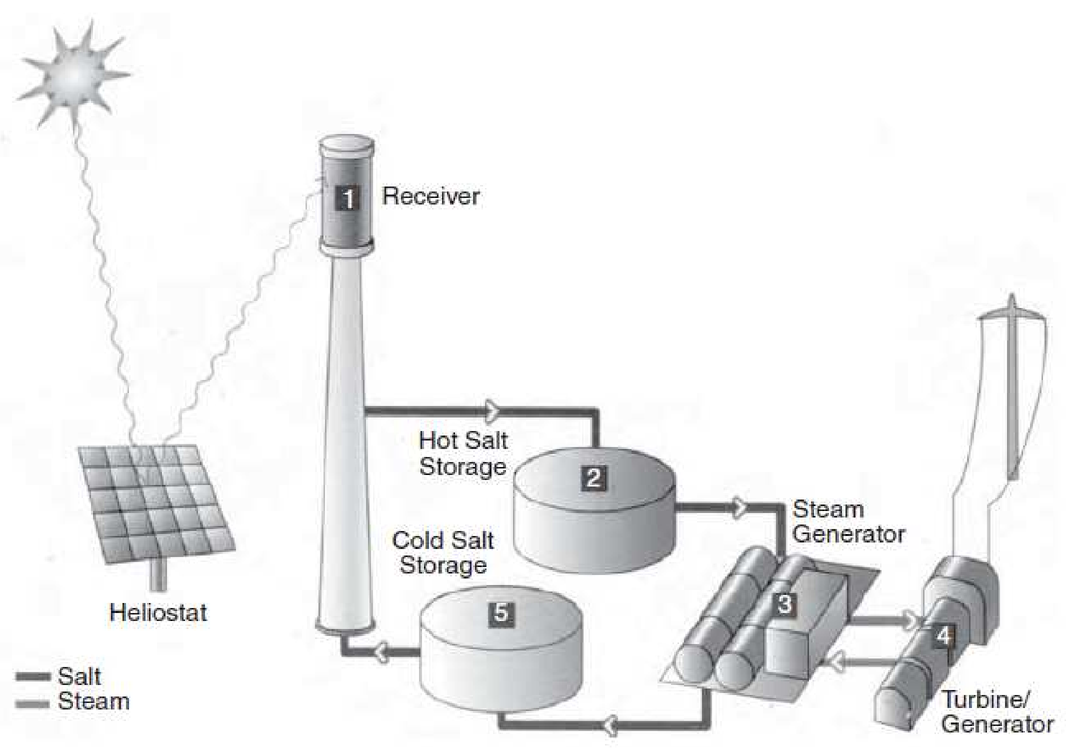

Fig.1.5: *Schematic representation of a solar thermal power station for generating electricity* [3].

In summary, hydroelectricity and wind are important contributors to the overall energy landscape. Wind, in particular, has seen remarkable growth over the past decade. It has been proposed that photovoltaic (PV) technologies could meet global energy consumption by covering about 0.4 % of the earth’s land area with solar cells having an efficiency of 10 %.

Inter alia, materials play an important role in determining the cost of a solar panel. Hence, the development of low cost solar materials that enable to improve the performances of photovoltaic devices is crucial to making solar energy a competitive and large-scale energy source.

I.3. Solar materials for photovoltaic application

The working principle of all today solar cells is essentially the same. It is based on the photovoltaic effect. In general, the photovoltaic effect means the generation of a potential difference at the junction of two different materials in response to visible or other radiation. The basic processes behind the photovoltaic effect are:

A. Generation of the charge carriers due to the absorption of photons in the materials that form a junction;

B. Subsequent separation of the photo-generated charge carriers in the junction;

C. Collection of the photo-generated charge carriers at the terminals of the junction.

In general, a solar cell structure consists of an absorber layer (Fig1.6), in which the photons of incident radiation are efficiently absorbed resulting in the creation of electron-hole pairs.

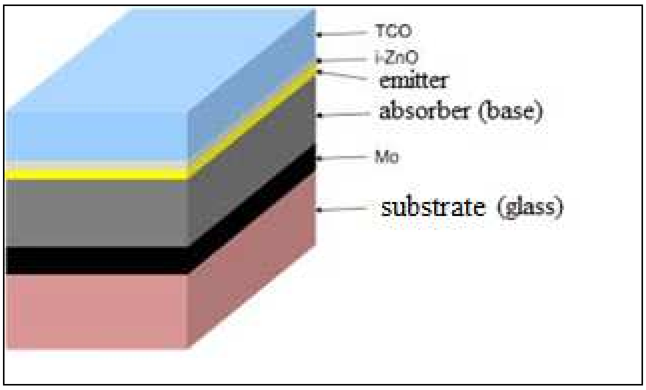

Fig.1.6: *Schematic illustration of general architecture of solar cell device.*

Based on the absorber type we can distinct several technologies of solar cells. Table 1.1 summarizes several types of solar cells. However, Table 1.2 gives the properties of frequently used solar materials as solar cell absorber layers.

Table 1.1
Foremost types of solar cells [8].

Type	**Efficiency (%)**	**Cost ($/Wp)**	**Market share (%)**
Monocrystalline Si	17-20	3.0	30
Polycrystalline Si	15-18	2.0	40
Amorphous Si	5-10	1.0	5
CIGS	11-13	1.5	5
CdTe-CdS	9-11	1.5	10

Table 1.2
Physical properties of principle solar cell materials [8].

Material	**Ge**	**$CuInSe_2$**	**Si**	**GaAs**	**CdTe**
Type of gap	Indirect	Direct	Indirect	Direct	Direct
Band gap (eV)	0.67	1.04	1.11	1.43	1.49
Absorption edge (µm)	1.85	1.19	1.12	0.87	0.83
Absorption coefficient (cm^{-1})	5.0×10^4	1.0×10^5	1.0×10^3	1.5×10^4	3.0×10^4

The crystalline silicon solar cell was the first practical solar cell invented in 1954. The efficiency[2] of silicon-based solar cells is in the order of 15 - 20 %, which is still the highest in single-junction solar cells [8].

Up to now, silicon still accounts for more than 75 % of the solar cell market. There are two variants of the crystalline silicon solar cell: mono-crystalline and polycrystalline. Amorphous silicon thin-film silicon solar cells are much less expensive than the crystalline ones. However, the efficiency is only about 5 - 10 % [8].

CIGS[3] and CdTe thin film solar cells, with a typical efficiency of around 10 % and account for about 15 % of the market. Because of the very absorption coefficient, a little amount of materials is required, thus; the unit price per peak-watt is lower than crystalline silicon solar cells.

To date, organic solar cells still have low efficiency and a short lifetime, and the market share is insignificant.

I.3.1. Silicon based solar cells

The first invented practical solar cell based on the crystalline silicon. The material has many advantages [8]:

- Silicon is an abundant material. It is the second most abundant element after oxygen, comprises 27 % of Earth’s crust;
- Its band gap is almost optimum for photovoltaic conversion regarding the solar spectrum;
- Silicon is very stable from chemical point of view;
- Due to the development of the microelectronics industry; the production and processing of ultrapure silicon are well developed;

---

[2] Efficiency is defined as, the ratio of energy output from the solar cell, to input energy from the sunlight [8].
[3] Abbreviation of "Copper (indium, gallium) selenium" based solar cells.

- After more than half a century of research and development, the efficiency of silicon solar cells reaches 24.7 % for research prototypes, which is already close to its theoretical limit.

I.3.2. Thin-film solar cells

Silicon has the lowest absorption coefficient compared to other solar materials (see Table 1.2); therefore, a thick substrate is required. The minimum thickness to maintain reasonable absorption and mechanical strength is 0.1 - 0.2 mm [8]. The wafer is cut from a mono-crystalline or polycrystalline ingot, therefore, the cost of the material and mechanical processing influence on the cost of the Si-based solar cells.

To rid this problem, thin film technology is an important alternative. Amorphous silicon thin-film solar cells; due to their relatively low efficiency, are tolerable for low-efficiency applications.

The direct semiconductors frequently have absorption coefficients higher than silicon; see Table 1.2. For those materials, a thickness of a few micrometers is sufficient. Currently, tow main technologies have reached the status of mass-production, namely; Cadmium Telluride "CdTe" and Copper (Indium-Gallium) Selenium "Cu(In, Ge)Se" often abbreviated as CIGS [8]. However, CZTX solar materials are emerging as very credible and attractive technology for thin film based solar cells.

In practice, there are many factors which determine the reasonableness of making thin-films based solar cells, such as; the reduction of the cost of the devices, environmental aspect, the use of flexible structures…etc.

I.3.2.1. Amorphous silicon based solar cells

Because the cost of some constituents of CdTe and CIGS solar materials, especially, tellurium and indium, for low-efficiency applications; such as hand-held calculators and utility-scale photovoltaic fields in deserts, silicon thin-film solar cells have been mass-produced for many years. Furthermore, silicon thin-film solar cells can be manufactured on flexible substrates [8].

The low absorption coefficient is the foremost disadvantage of silicon. Nevertheless, doping amorphous silicon with hydrogen up to 10 % may increase its absorption coefficient until 10^5 cm^{-1}, with a band gap of 1.75 eV. This material is habitually abbreviated as a-Si:H [8, 9]. Due to the high defect density; the recombination rate in high, as a result, the reached-efficiency of the best experimental a-Si:H solar cells, is around 10 % [8]. The mass-produced for a-Si:H solar cells is around 5 % (see Table 1.1).

I.3.2.2. CdTe based Solar Cells

Due to its high absorption coefficient and simplicity in making a p-type material, cadmium telluride (CdTe) is currently the most widespread material for thin-film solar cells [9]. Moreover, CdTe exhibits a compatibility with CdS; a wide-band gap semiconductor for which it is feasible to manufacture an n-type film, because the absorption edge of CdS is 2.4 eV, it is transparent to the bulk of solar radiation [8].

The typical construction of a CdTe solar cell is shown in Fig.1.7. The solar cell device is made of a 5 μm film of CdTe, covered with a 100 nm CdS thin film, to form a pn-junction. To the sunny side is a film of TCO (transparent Conducting Oxide); to allow radiation to come in and serves as a conductor. However, to the back side is a metal film for electric contact, a 0.5 mm EVA (Ethylene-Vinyl acetate) film is added for mechanical protection. The best efficiency of CdTe based solar cells is 16.5 % and expected to reach 20 % [8].

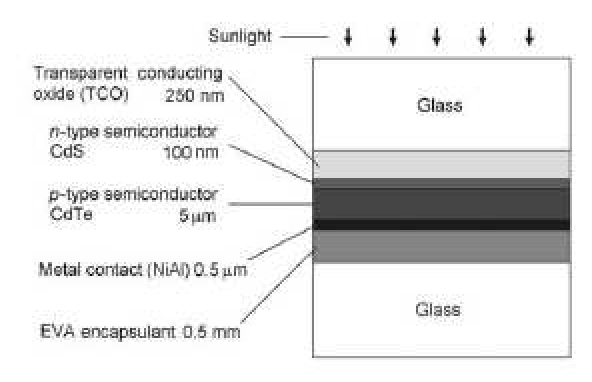

Fig.1.7: *Typical structure of CdTe thin-film solar cell* [8, 9].

A major question often asked is on the subject of the toxicity of cadmium. According to a recent study, the environment impact may be neglected; because the used amount of cadmium is very small and is completely sealed by glass.

I.3.2.3. CIGS based Solar Cells

The $CuInSe_2$-CdS system was discovered in 1974 as a photovoltaic light detector [8, 10]. In 1975, CIGS-based solar cell was built, which showed efficiency comparable to the silicon solar cells at that time [8, 11].

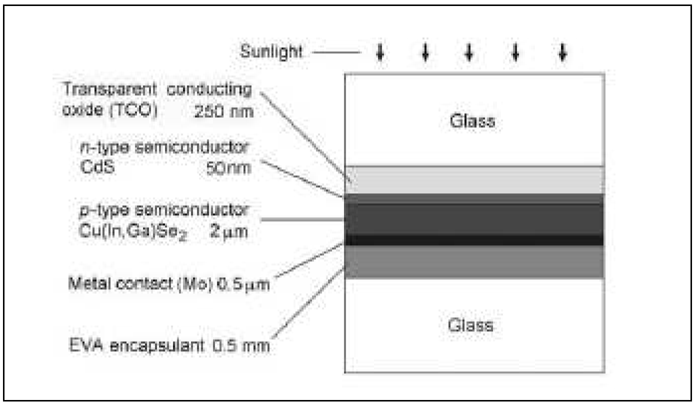

Fig.1.8: *Typical structure of CIGS thin-film solar cell* [8, 10].

At the beginning of the 21st century, the efficiency of CIGS thin-film solar cells has reached 19.9 %; which is comparable to polycrystalline silicon solar cells [9]. The absorption coefficient of CuInSe is about 100 times greater than silicon. Thus, with a 2-µm thin film of this semiconductor, more than 90 % of the near infrared and visible light would be absorbed [8].

The typical structure of a CIGS solar cell is shown in Fig.1.8. Similar to the CdTe solar cells; a 50 nm n-type CdS film is used to form a pn-junction, also, the environment impact is negligible; because the used amount of cadmium here is very small and sandwiched between two glass plates [8].

Fig.1.9: *An experimental CIGS solar cell integrated circuit. The nominal voltage of each CIGS solar cell is 0.5 V. By connecting 10 individual CIGS solar cells in series internally; a 5 V solar cell is built. Because the connections are integrated, the device is compact and rugged* [8].

The CIGS solar cell may well be produced by a wet process; without requiring a vacuum. Therefore, the manufacturing cost can be cushioned. The interconnections between CIGS solar cells can be made on the same structure, similar to an integrated circuit, thus a higher voltage single cell can be made without requiring external connections. Fig.1.8 illustrates an experimental "5 V" CIGS solar cell; made from 10 individual CIGS solar cells in a single-glass envelop [8].

I.3.2.4. CZTX based Solar Cells

CZTX have attracted much attention due to its use in cost effective fabrication of thin film solar cell and its nontoxic constituting elements. CZTX are promising materials due to their energy gap of 1 eV in the case of Se-based compound and 1.5 eV for S-based compound, which is the optimum band gap for use as an absorber layer in solar cell devices [12].

The absorption coefficient of CZTX solar materials is around 10^4 cm^{-1} in the visible region, which is also reasonable. Thus, because of its good material properties for solar cell device applications as well as economic and environmental advantages; CZTX is regarded as alternative photovoltaic (PV) technology to CdTe and Cu(In,Ga)(S,Se) abrivied (CIGS).

Fig.1.10 illustrates a typical structure of a CZTX solar cell. The device is made of a 2 μm film of CZTX "p-type", covered with a 50-70 nm CdS "n-type" thin film, to form a pn-junction. To the sunny side is a transparent film of AZO (aluminum-doped zinc oxide) behaves as window for radiation and conductor with an Aluminum grid. To the back side is a metal film for electric contact. SLG (Soda-Lime Glass) or polyimide film is added for mechanical protection.

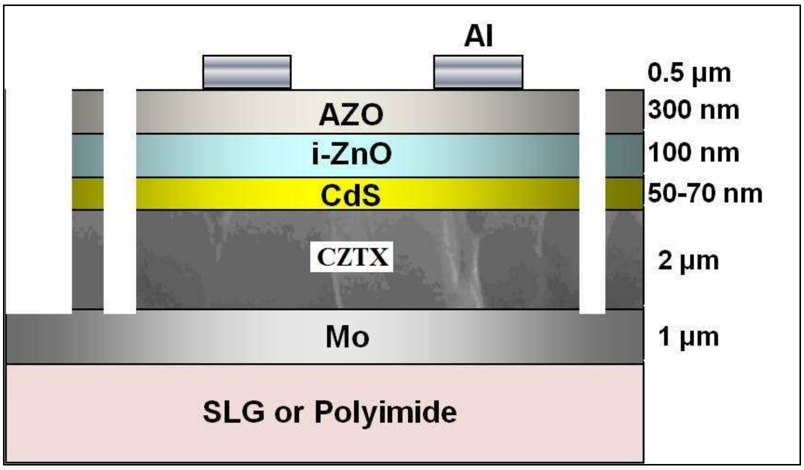

Fig.1.10: *Typical structure of CZTX thin-film solar cell.*

The conversion efficiency of CZTX related solar cell devices has been steadily improved during the last decade [12- 17], and recently an efficiency of 10.1 % was achieved for a mixed sulfo-selenide device using a hydrazine- based solution deposition approach [12 , 18]. An efficiency of up to 8.4 % has been achieved for pure sulfide sputtered CZTS devices [19].

I.4. CZTX alloys as attractive solar materials for photovoltaic application

I.4.1. CZTX-based solar cells

The field of CZTX solar cells is young; nevertheless, it represents veritable potential solar materials for photovoltaic solar energy application. We summarize their foremost advantages:

- These materials contain abundant, inexpensive and non-toxic elements that lead to less environmental damage and low cost devices, which are the main challenges for the photovoltaic solar energy development.
- They are desired in photovoltaic for their properties such as direct-band gap, high absorption coefficient (about $10^{-4}cm^{-1}$), and possess optimal band gap energy of 1-1.5 eV.
- Flexibility is needed in certain solar cells applications, then these technologies (CZTX (X=S and Se)) may be favored.
- Bas du formulaire
- CZTX have relative low temperature coefficients compared to silicon, CdTe and $Cu(In,Ga)Se_2$ thin film based solar cells; Thus, CZTX based solar cells show a great potential in photovoltaic applications in hot environments.

In the context of the last point, we have demonstrated [20] that; the quaternary semiconductor CZTSSe has low temperature coefficients (dI_{sc}/dT, dV_{oc}/dT *and* $d\eta/dT$) compared to silicon, CdTe and CIGS based solar cells.

We summarize the analysis of the performed comparative study on the behavior of solar cells under thermal gradient in the following section.

I.4.2. Solar cells behavior under thermal gradient

Table 1.3 shows the values of dI_{sc}/dT, dV_{oc}/dT and $d\eta/dT$ of single crystalline, polycrystalline silicon and thin film solar cells. In this section, we are typically interested in the photovoltaic conversion efficiency η because it is the most important factor for describing the performances of any photovoltaic device.

The analysis of temperature effect on the conversion efficiency shows that silicon technology has larger temperature coefficient, this leads to a problem in exploitation of silicon based solar cells in hot regions where solar irradiation is important, *i.e.* high temperatures, for photovoltaic applications. So, it is recommended to adopt other technologies for hot environments.

Both technologies, CdTe and Cu(In,Ga)Se cannot be good alternatives for silicon technology, in particular in terrestrial applications; the first contains a toxic element (cadmium), the second contains expensive rare metals (indium and gallium). However, the quaternary semiconductor CZTSSe contains abundant, cheaper and nontoxic elements. In addition, it has a low temperature coefficient. Thus, CZTSSe solar cells show a great potential in photovoltaic applications in hot environments.

Table 1.3

Temperature coefficients of I_{sc}, V_{oc} and η.

Technology	Silicon			Other compounds		
	Polycrystalline		Single crystalline	Cu(In,Ga)Se [21]	CZTSSe [17]	CdTe [22]
Temperature coefficients	[20]	Literature				
dI_{sc}/dT (mA/K)	2.1	2.38[a]	1.75[a]	-	-	-
dV_{oc}/dT (mV/K)	-2.1	[-2.3, -2.2][b]		[-3.3, -2.01]	-1.91	[-2.2, -2.1]
$d\eta/dT$ ($\%/K$)	-0.063	-0.042[b]		[-0.064, -0.017]	-0.013	-

[a]: Reference [23].

[b]: Reference [24].

I.5. Summary

We have presented in this introductory chapter some arguments about the need of renewable energy including climatic changes dilemma and energy demand increasing. Therefore, renewable energy is becoming an optimal solution of these universal problems; we talked about some renewable energy resources including hydroelectric, wind power and solar energy. Then we have talked about materials for solar energy applications (absorbers), and we have cited the main technologies, such as, silicon based solar cells, cadmium telluride (CdTe) and copper indium-gallium sulphide-selenide (CIGS) based thin films solar cells, and we focused on our studied solar materials *i.e.* CZTX alloys as attractive solar materials for photovoltaic conversion. Furthermore, we discussed the validity and performances of CZTX-based solar cells under thermal gradient effect compared to other main technologies *i.e.* Silicon, CdTe and CIGS based thin films solar cells.

References

[1] N. S. Lewis, MRS Bull. 32 (2007) 808.

[2] Worldwatch Institute (May 2014), *Use and Capacity of Global Hydropower Increases*, available on line: http://www.worldwatch.org/node/9527 (May, 23rd 2014).

[3] M. R. Patel, Wind and Solar Power Systems: Design, Analysis, and Operation, 2 edition, CRC Press, Boca Raton, FL, 2005.

[4] N. Stauffer, *Catch the wave*, MIT Tech Talk, 53 (2008) 4.

[5] REN21 Renewables 2010 Global Status Report, Deutsche Gesellschaft für Technische Zusammenarbeit (GTZ) GmbH, Paris, 2010.

[6] J. Callaghan, Future Marine Energy, Carbon Trust, UK, 2006.

[7] A. Demirbas, Appl. Energy 86, Supplement 1 (2009) S108.

[8] C. J. Chen, Physics of Solar Energy, John Wiley & Sons, Inc., Hoboken, New Jersey, 2011.

[9] K. L. Chopra, P.D. Paulson, V. Dutta, Prog. Photovolt. Res. Appl. 12 (2004) 69.

[10] S. Wagner, J.L. Shay, P. Migliorato, H.M. Kasper, Appl. Phys. Lett. 25 (1974) 434.

[11] J. L. Shay, S. Wagner, H.M. Kasper, Appl. Phys. Lett. 27 (1975) 89.

[12] T. K. Todorov, K.B. Reuter, D.B. Mitzi, Adv. Mater. 22 (2010) E156.

[13] H. Katagiri, K. Jimbo, W. S. Maw, K. Oishi, M. Yamazaki, H. Araki, A. Takeuchi, Thin Solid Films 517 (2009) 2455.

[14] D. B. Mitzi, O. Gunawan, T. K. Todorov, K. Wang, S. Guha, Sol. Energy Mater. Sol. Cells 95 (2011) 1421.

[15] M. A. Green, K. Emery, Y. Hishikawa, W. Warta, Prog. Photovolt. Res. Appl. 18 (2010) 346.

[16] B. A. Andersson, Prog. Photovolt. Res. Appl. 8 (2000) 61.

[17] J. Krustok, R. Josepson, M. Danilson, D. Meissner, Sol. Energy 84 (2010) 379.

[18] D. A. R. Barkhouse, O. Gunawan, T. Gokmen, T. K. Todorov, D.B. Mitzi, Prog. Photovolt. Res. Appl. 20 (2012) 6.

[19] B. Shin, O. Gunawan, Y. Zhu, N. A. Bojarczuk, S. J. Chey, S. Guha, Prog. Photovolt. Res. Appl. 21 (2013) 72.

[20] S. Bensalem, M. Chegaar, M. Aillerie, Energy Procedia, 36 (2013) 1249.

[21] R. Kniese, D. Hariskos, G. Voorwinden, U. Rau, M. Powalla, Thin Solid Films 431–432 (2003) 543.

[22] J. E. Phillips, W.N. Shafarman, E. Shan, in:, IEEE Photovolt. Spec. Conf. - 1994 1994 IEEE First World Conf. Photovolt. Energy Convers. 1994 Conf. Rec. Twenty Fourth, 1994, pp. 303–306 vol.1.

[23] W. De Soto, S. A. Klein, W.A. Beckman, Sol. Energy 80 (2006) 78.

[24] P. Singh, S. N. Singh, M. Lal, M. Husain, Sol. Energy Mater. Sol. Cells 92 (2008) 1611.

Chapter II

Theoretical Study of Fundamental Properties of CZTX (X=S and Se)

II.1. Preamble

In this chapter we cite and discus the main part of this work which focuses on the theoretical study of physical properties of CZTX solar materials. Firstly, we expose foremost previous theoretical works dealing with CZTX solar materials; especially those that concern the electronic properties and the estimation of the gap value, the optical properties and the absorption coefficient, then we talk about our contribution which focuses on the structural, mechanic and thermodynamic properties of CZTX solar materials. A thorough description of the calculation scheme is also given in the end of this chapter.

II.2. Previous works on fundamental properties of CZTX solar materials

In the literature several theoretical works discussed the fundamental properties of CZTX. We cite the most important contributions, as follows; Chen et al [1] calculated the crystal and electronic band structure of CZTX with VASP code. Persson [2] calculated the electronic and optical properties of CZTX using WIEN2K code. Botti et al [3] calculated systemically the band structures of CZTX by means of many-body methods. We explain the contributions of these authors, considering the electronic structure and the optical properties of CZTX alloys.

II.2.1. Electronic properties

II.2.1.1. Estimation of the gap value

All cited works show that the use of both LDA and GGA approximations to study the electronic structure and to evaluate the gap of the concerned compounds is totally an inadequate approach [3] that is what we found also for both compounds. The calculated LDA and GGA band gaps of CZTX compounds are illustrated in the Table 2.1.

Table 2.1

Calculated gap value for CZTX solar materials using LDA and GGA.

	Sulphide compound				**Selenide compound**			
Absorber	KS-CZTS		ST-CZTS		KS-CZTSe		ST-CZTSe	
Approximation	LDA	GGA	LDA	GGA	LDA	GGA	LDA	GGA
E_g *(eV)*	0.012	0.342	0.000	0.212	0.026*	0.007*	0.000	0.016

* Reference [4].

Therefore, to obtain a reasonable gap value the use of other approaches otherwise standard LDA and GGA is indispensable.

In this purpose, Persson [2] has used an optimized GGA+U as exchange correlation potential. Chen et al [1] have performed hybrid functional calculations (HSE06) using experimental lattice constants. For Botti et al contribution [3]; the calculations are based on a restricted self-consistent (sc) GW scheme.

The study of Persson is based on the relativistic FPLAPW method [5] using the generalized gradient approximation GGA of Engel and Vosko [6] plus an onsite Coulomb interaction U_d for the *d*-states. The considered GGA potential has been demonstrated to generate accurate gamma-point effective masses [7, 8].

In the framework of GGA+U approach, Person used an eight atoms body-centered primitive cell with $U_d(Cu, Zn)$=4 eV and $U_d(Sn)$=6 eV. The used GGA+U method is optimized for obtaining a good exchange-correlation potential to obtain better electronic structures and accurate values of gap energy.

Botti et al through their contribution [3] solved the gap value estimation problem for these materials; authors used a restricted self-consistent (sc) GW scheme to determine accurate quasi-particle band structures of both kesterite and stannite CZTX solar materials.

The exploited (scGW) consists in performing a self-consistent GW calculation within the Coulomb hole plus screened exchange approximation followed by a perturbative GW on top of it [3, 9]. It is noted that, this method has been applied to various transition-metal based compounds, where excellent results for the band gaps estimation and the quasi-particle band structure have been reported [10-12].

In Fig.2.1, the *scGW* band structures for CZTX compounds considering both KS and ST types are illustrated. The estimated band gaps are in remarkable agreement with experimental results. The S-based compounds have a greater gap compared to the Se-based ones; in addition, kesterites exhibit consistently greater gaps than stannites [3].

As it is well known, the LDA and GGA underestimate the band gaps, Chen et al [1] have performed hybrid functional calculations (HSE06) using experimental lattice constants, where 25 % of the GGA exchange potential is replaced by screened Fock exchange.

The following table (Table 2.2) summarizes the obtained gap value from the explained theoretical contributions. Thus, from Table 2.2, the mentioned studies give similar results. Consequently, the mentioned methods yield fairly accurate band-gap energies. It is noted that, for better study of the electronic and optical properties of the absorbers; it is very important to obtain improved band structure.

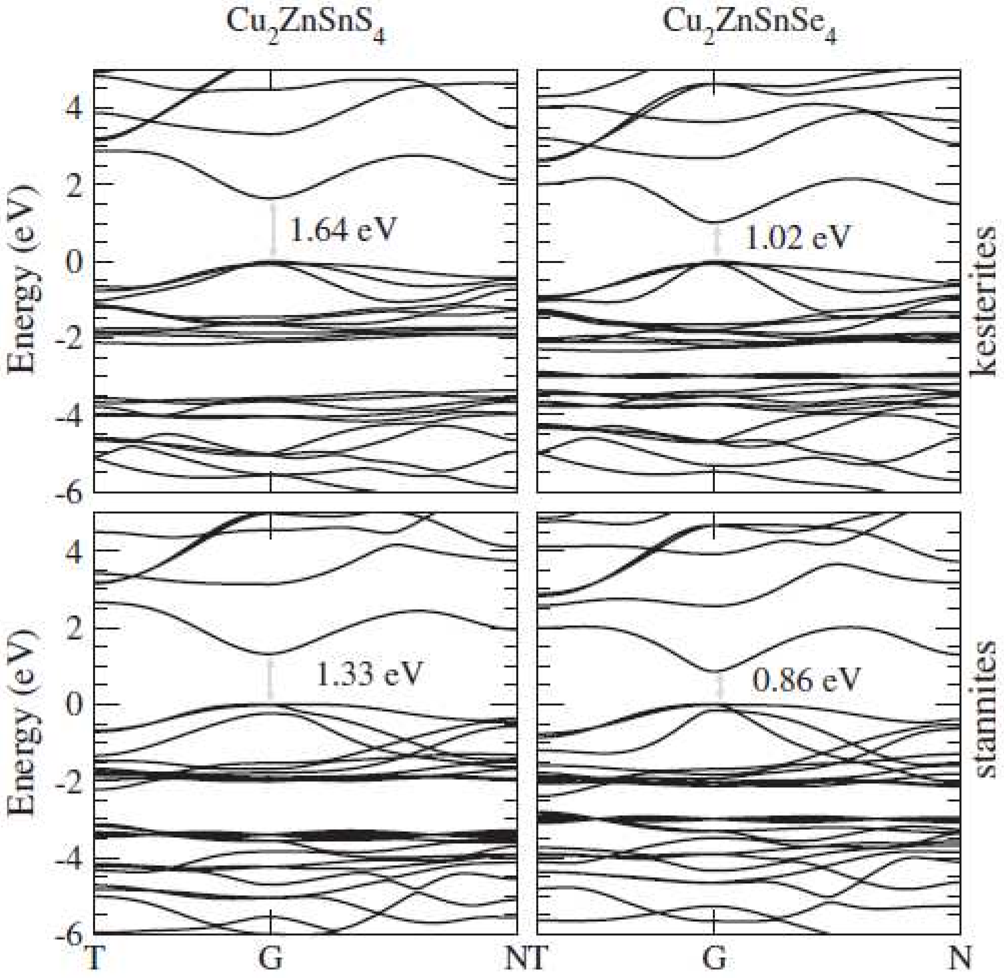

Fig.2.1: *Band structures from scGW approach for kesterite and stannite CZTX solar materials. Top valence bands are set to zero* [3].

Table 2.2

Calculated gap value of CZTX solar materials from literature compared to the available experimental data.

Compound	Structure type	Calculated gap (eV)	Experiment
CZTS	KS	1.56[a]; 1.50[b]; 1.64[c]	1.4–1.6 [4]
	ST	1.42[a]; 1.38[b]; 1.33[c]	0.8–1.0 [5]
CZTSe	KS	1.05[a]; 0.96[b]; 1.02[c]	1.4–1.5 [6]
	ST	0.89[a]; 0.82[b]; 0.86[c]	0.8–1.0 [5]

[a] Reference [2]; [b] Reference [1]; [c] Reference [3].

II.2.1.2. Partial and total density of states

Chen et al [1] calculated the total density of states (DOS) of CZTS for the KS and ST types and the partial DOS for the KS type, the calculated results are shown in Fig.2.2.

From the calculated partial DOS, the upper valence band is derived mainly from the hybridization of S p and Cu d states, that which is similar to $CuInSe_2$ and $CuGaSe_2$; because Cu has higher d orbital energy than Zn, Ga, In, and Sn, whereas the low conduction band is mainly derived from the hybridization of S s, p and Sn s states, and this is due to the lower s orbital energy of Sn than the other cations [1].

The total DOS has similar shape for KS and ST structure types, which indicates that the dependence of the band structure on the distribution of Cu and Zn; and consequently on the type of CZTX compounds, is weak for this class of materials [1].

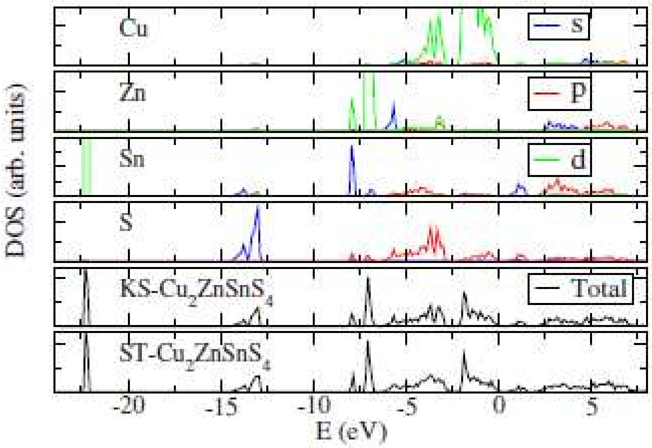

Fig.2.2: *The total DOS of CZTS for the KS and ST types and the partial DOS for the KS type* [1].

II.2.2. Optical properties

II.2.2.1. Dielectric function

The optical properties may be evaluated from the knowledge of the complex dielectric function $\varepsilon(\omega)=\varepsilon_1(\omega)+i\varepsilon_2(\omega)$. The four compounds have all rather similar dielectric function [2]; as shown in Fig.2.3.

The beginning to the response of the imaginary part of the dielectric function is due to the band-gap energy; around of this beginning, the stannite type show strong anisotropy $\varepsilon_2^{\perp}(\omega \approx E_g/\hbar) > \varepsilon_2^{\parallel}(\omega \approx E_g/\hbar)$ compared to the kesterite type, for both compounds.

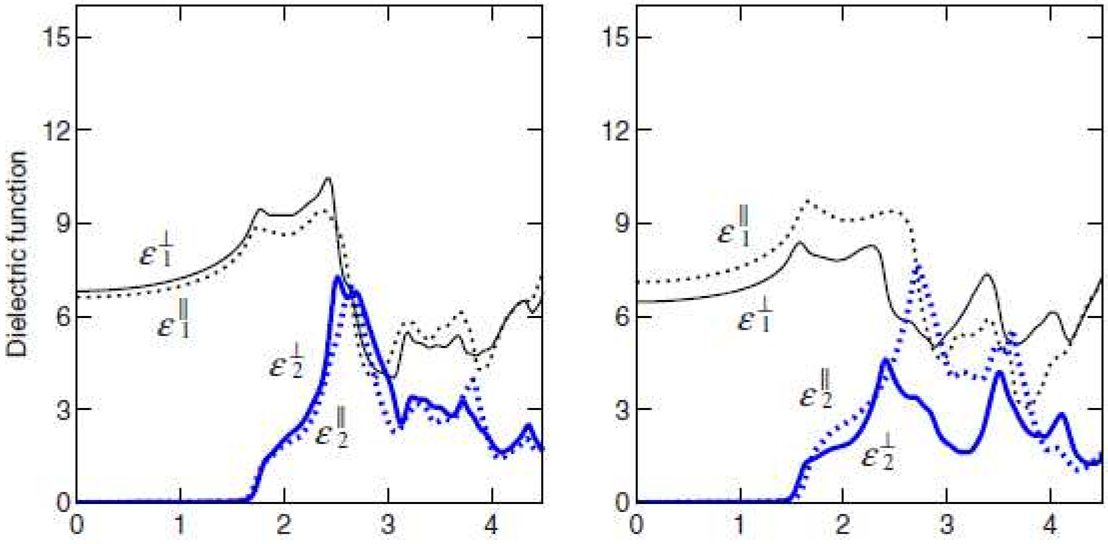

(a) Kesterite Cu_2ZnSnS_4

(b) Stannite Cu_2ZnSnS_4

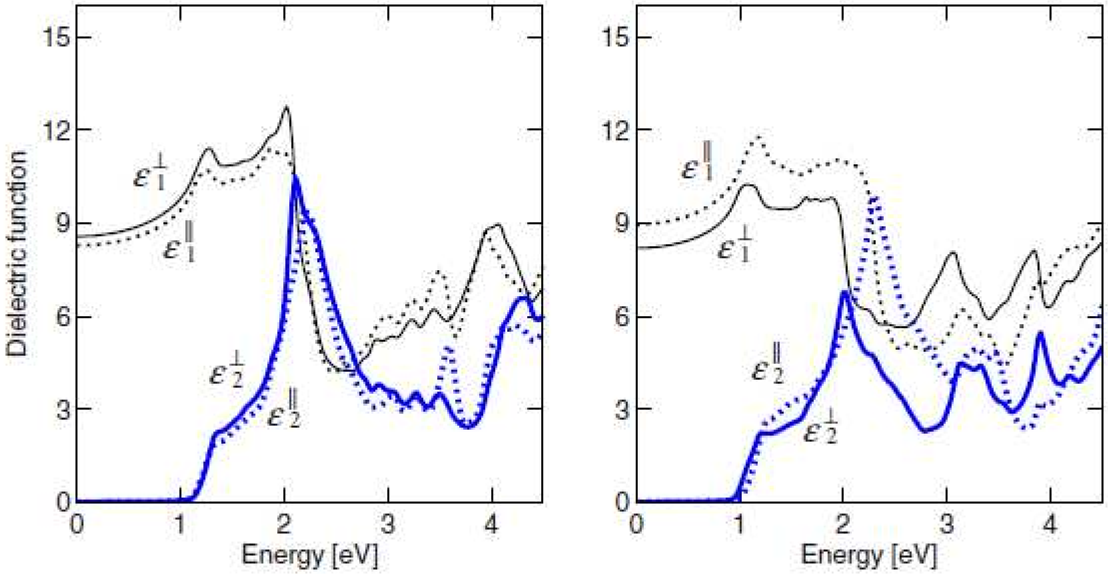

(c) Kesterite $Cu_2ZnSnSe_4$

(d) Stannite $Cu_2ZnSnSe_4$

Fig.2.3: *The dielectric function* $\varepsilon(\omega)=\varepsilon_1(\omega)+i\varepsilon_2(\omega)$ *of CZTX solar materials. The thin black lines represent the real part* $\varepsilon_1(\omega)$ *and the thick blue lines represent the imaginary part* $\varepsilon_2(\omega)$*. Also, the dielectric function is divided into the transverse contribution* $\perp$ *(solid lines) and longitudinal contribution* $\|$ *(dotted lines)* [2].

At rather larger energies *i.e.* in the interval about 1.5-2.0 eV; opposite anisotropy appears for the stannite type $\varepsilon_2^{\perp}(\omega) < \varepsilon_2^{\parallel}(\omega)$ for both compounds, however, $\varepsilon_2^{\perp}(\omega) > \varepsilon_2^{\parallel}(\omega)$ for kesterite type.

The dielectric functions of all four concerned compounds exhibit a strong $\varepsilon_2(\omega)$ peak at about 2.0-2.5 eV, and this peak is more evident in the case of the kesterite type for both compounds, whereas; the two stannite-type compounds demonstrate much stronger anisotropy of their response peaks.

Likewise, the anisotropy reflects in the real part $\varepsilon_1(\omega)$ of the dielectric function. At low energies *i.e.* about 2.0 eV; $\varepsilon_1^{\perp}(\omega) > \varepsilon_1^{\parallel}(\omega)$ in the case of the kesterite type for both compounds, while, the reverse is true for the tow stannite compounds *i.e.* $\varepsilon_1^{\perp}(\omega) < \varepsilon_1^{\parallel}(\omega)$.

The estimated values of high-frequency dielectric constant ε_∞ for the studied solar materials are illustrated in Table 2.3. The Se-based compounds show larger ε_∞ compared to S-based ones; and this in consistency with the values of band gap. Note that, both considered types, for both materials show rather comparable values of ε_∞.

Table 2.3

Calculated high-frequency dielectric constant $\varepsilon_\infty \equiv \varepsilon_1\left(0 \ll \omega \ll E_g/\hbar\right)$ in the transverse and longitudinal directions [2].

	Sulphide compound		**Selenide compound**	
Absorber	KS-CZTS	ST-CZTS	KS-CZTSe	ST-CZTSe
$\varepsilon_\infty^{\perp}$	6.8	6.5	8.6	8.2
$\varepsilon_\infty^{\parallel}$	6.6	7.1	8.3	9.0

II.2.2.2. Absorption coefficient

The absorption coefficient α represents the linear optical response from the valence bands to the lowest conducting bands [2]. The absorption is directly deduced from the dielectric function [2, 13]. Consequently, all CZTX solar compounds have comparable absorption coefficient.

Fig.2.4 below shows the calculated absorption coefficients for the KS-CZTX solar materials by Persson [2]. The difference in the onset of the absorption is due to the difference in the band-gap energy of the concerned materials.

The calculated absorption coefficient for the KS-CZTS by Persson [2] is in agreement with experimental reported data in the literature [14-17] which have shown that; kesterite CZTS has a band edge absorption coefficient more than 10^4 cm^{-1}.

The absorptions of KS-CZTX are similar to that of $CuInSe_2$ (CISe), nevertheless in the energy region around 1.5 eV the onset of the absorption is much stronger for the KS-CZTX than CISe. For higher energies; about 2.5-3.0 eV, the absorptions of KS-CZTX compounds decrease whereas the absorption of CISe shows an increasing.

It is noted that, Persson [2] considered the direct transitions only to calculate the absorption coefficient, however, at high temperatures phonon assisted transitions will be an additional contribution that will somewhat extend the spectra.

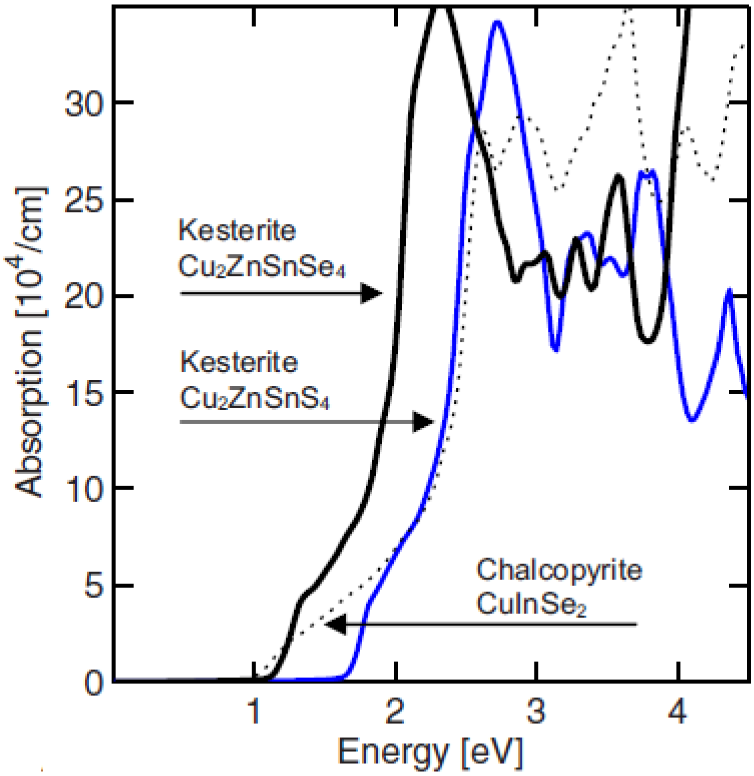

Fig.2.4: *Absorption coefficients of kesterite CZTX solar materials. For comparison, the absorption coefficient of chalcopyrite CISe is also presented* [2].

II.2.3. Mechanical and thermodynamic properties

On the theoretical side, few works were interested with mechanical and thermodynamic fundamental properties of absorber solar materials. For the considered herein CZTX solar materials, the recent contributions of He and Shen [18, 19] presented a study of some mechanical and thermo-physical properties of kesterite-type Cu_2ZnSnX_4 using Vienne ab initio simulation package.

They have evaluated for kesterite-type CZTX: the elastic constants and elastic moduli at zero pressure condition, the B/G ratio which indicates that the kesterite-type CZTX compound is prone to ductile behavior and some thermodynamic parameters that are : the entropy (S), the vibrational energy (A), the internal energy (U) and Gibbs energy (G).

The calculated results of He and Shen [18, 19] will be compared with our obtained results; especially for the mechanical parameters concerning the KS type of CZTX.

II.3. Our contribution about CZTX solar materials physical properties

Most theoretical works on CZTX solar material compounds considered electronic and optical properties. Few works have dealt with mechanic and thermodynamic properties of these alloys *vs.* their different phases.

Despite much earlier efforts, our understanding of fundamentals properties, especially, mechanical and thermodynamic properties and their behavior under external disturbance pressure and temperature is still far from satisfactory.

To the best of our knowledge, studies on the mechanical and thermodynamic properties of ST-type of CZTX have not been reported in the literature. Therefore, in this work we would like to provide information regarding ST-CZTX structural, mechanical and thermodynamic properties for eventual photovoltaic technological applications.

Another primordial reason that makes our contribution meaningful; resides in the fact that energy difference between KS (space group $I\bar{4}$) and ST type (space group $I\bar{4}2m$) is small (few meV/atom) [1, 3], accordingly; both structures can coexist in synthesized samples. In fact, a comparative investigation of the physical properties of both types for both alloys is very significant; in other words, necessary.

Therefore, the aim of this work is to provide further information concerning mainly the elastic and thermodynamic properties of CZTX as novel photovoltaic solar material absorbers for both KS and ST types, and then to take advantage of the properties of CZTX for thin films based solar cells, for eventual photovoltaic technological applications.

II.4. Detail of calculations

In this study, all the computations have been done by the use of the Cambridge Serial Total Energy Package CASTEP code [20]. In this code, the Kohn-Sham equations are solved within the framework of density functional theory [21, 22] by expanding the wave functions of valence electrons in a basis set of plane waves with kinetic energy smaller than a specified cut-off energy.

Interactions of electrons with ion cores are represented by the Vanderbilt-type ultrasoft pseudo-potential [23]. The states Cu 3d10 4s1, Zn 3d10 4s2, Sn 5s2 5p2, S 3s2 3p4, Se 4s2 4p4 were treated as valence states. The electronic exchange correlation interactions are treated within the Wu-Cohen generalized gradient approximation (GGA-WC) [24, 25].

We used a plane-wave basis set defined by an energy cut-off 400 eV. The Brillouin zone sampling was carried out using 75 k-points in the irreducible part, which correspond to 5×5×6 and 6×6×7 set of Monkhorst-Pack points [26] for KS and ST structure respectively.

The structural parameters are determined using the Broyden-Fletcher-Goldfarb-Shenno (BFGS) minimization technique [27]. The system reaches the ground state via self consistent calculation when the total energy is stable within 5×10^{-6} eV/atom, the displacement of atoms during the geometry optimization is less than 5×10^{-4} Å, the maximum ionic Hellmann-Feynman force is less than 10^{-2} eV/Å, and the maximum stress is within 2×10^{-2} GPa.

The elastic coefficients were determined by applying a set of given homogeneous deformations with a finite value and calculating the resulting stress with respect to optimizing the internal atomic freedoms [28]. The criteria for convergences of optimization on atomic internal freedoms were chosen as follows: the difference of total energy within 10^{-6} eV/atom, ionic Hellmann-Feynman force within 6×10^{-3} eV/Å, and maximum ionic displacement within 2×10^{-4} Å. The maximum strain amplitude was set to be 0.003 in the present theoretical investigation.

Phonon calculations are used to evaluate the temperature dependence of some thermodynamic functions *i.e.* the entropy, free energy, internal energy and lattice heat capacity for both considered types of CZTX crystals in the framework of quasi-harmonic approximation.

CASTEP code allows us to perform phonon calculation using finite difference method. In the finite difference scheme a super cell defined by cutoff radius in Å specifies the real space cutoff radius for dynamical matrix calculations. This introduced value of cutoff radius will be used to construct an appropriate super cell.

A larger cutoff radius produces more accurate results at the expense of longer calculation times. In the present theoretical study, we choose super cell defined with cutoff radius of 5 Å which construct a super cell with a volume which is 8 times the original cell.

II.5. Summary

We have approached in this chapter the theoretical investigation on physical properties of CZTX solar materials. We have cited principal previous works concerning theoretical studies of CZTX solar materials, especialy, the electronic and optical properties. We have brought out the main attempts to evalute the gap of those materials; where we have exposed three contrubutions, namely; the works of Chen et al, Persson and that of Botti et al. Concerning the dielectric function and the absorption coefficient, we have explained the calculated results of Persson. Then we have talked about our contribution that focuses on the mechanical and thermodynamic properties of CZTX materials. In the end of the chapter we have given the details of calculation scheme that have been used in our theoretical study.

References

[1] S. Chen, X. G. Gong, A. Walsh, S. H. Wei, Appl. Phys. Lett. 94 (2009) 041903.

[2] C. Persson, J. Appl. Phys. 107 (2010) 053710.

[3] S. Botti, D. Kammerlander, M. A. L. Marques, Appl. Phys. Lett. 98 (2011) 241915.

[4] S. Bensalem, M. Chegaar, D. Maouche, *Contribution to the study of structural and electronic properties of CZTSe quaternary semiconductor for photovoltaic applications*, Congrès Algérien de Mécanique, 25-28 November 2013, Mascara, Algérie.

[5] P. Blaha, K. Schwarz, G. K. H. Madsen, D. Kvasnicka, J. Luitz, *WIEN2K: An Augmented Plane Wave+Local Orbitals Program for Calculating Crystal Properties*, Karlheinz Schwarz Techn. Universität, Wien, Austria, 2001.

[6] E. Engel, S. H. Vosko, Phys. Rev. B 47 (1993) 13164.

[7] C. Persson, Appl. Phys. Lett. 93 (2008) 072106.

[8] C. Persson, R. Ahuja, B. Johansson, Phys. Rev. B 64 (2001) 033201.

[9] L. Hedin, S. Lundqvist, Solid State Phys. 23 (1970) 1.

[10] J. Vidal, S. Botti, P. Olsson, J. F. Guillemoles, L. Reining, Phys. Rev.Lett. 104 (2010) 056401.

[11] F. Bruneval, N. Vast, L. Reining, Phys. Rev. B 74 (2006) 045102.

[12] J. Vidal, F. Trani, F. Bruneval, M. A. L. Marques, S. Botti, Phys. Rev.Lett. 104 (2010) 136401.

[13] C. Ambrosch-Draxl, J. O. Sofo, Comput. Phys. Commun. 175 (2006) 1.

[14] K. Ito, T. Nakazawa, Jpn. J. Appl. Phys. 27 (1988) 2094.

[15] H. Katagiri, K. Saitoh, T. Washio, H. Shinohara, T. Kurumadani, S. Miyajima, Sol. Energy Mater. Sol. Cells 65 (2001) 141.

[16] T. Tanaka, T. Nagatomo, D. Kawasaki, M. Nishio, Q. Guo, A. Wakahara, A. Yoshida, H. Ogawa, J. Phys. Chem. Solids 66 (2005) 1978.

[17] K. Moriya, J. Watabe, K. Tanaka, H. Uchiki, Phys. Status Solidi C 3 (2006) 2848.

[18] X. He, H. Shen, Physica B 406 (2011) 4604.

[19] X. He, H. Shen, Phys. Scripta. 85 (2012) 035302.

[20] S. J. Clark, M. D. Segall, C. J. Pickard, P. J. Hasnip, M. J. Probert, K. Refson, M. C. Payne, Z. Kristallogr. 220 (2005) 567.

[21] P. Hohenberg, W. Kohn, Phys. Rev. B 136 (1964) 864.

[22] W. Kohn, L.J. Sham, Phys. Rev. A 140 (1965) 113.

[23] D. Vanderbilt, Phys. Rev. B 41 (1990) 7892.

[24] Z. Wu, R. E. Cohen, Phys. Rev. B 73 (2006) 235116.

[25] F. Tran, R. Laskowski, P. Blaha, K. Schwarz, Phys. Rev. B 75 (2007) 115131.

[26] H. J. Monkhorst, J. D. Pack, Phys. Rev. B 13 (1976) 5188.

[27] T. H. Fischer, J. Almlof, J. Phys. Chem. 96 (1992) 9768.

[28] V. Milman, M. C. Warren, J. Phys.: Condens. Matter 13 (2001) 241.

Chapter III

Results and Discussion

III.1. Preamble

This chapter is consecrated to exhibit and discuss the obtained results. Firstly, we evaluate the structural parameters; we study at zero pressure the structural lattice constants and we present the hydrostatic pressure effect on the unit cell volume for the four CZTX considered solar materials in order to construct the Birch-Murnaghan equation of state. Then we discuss the elastic properties of CZTX compounds *i.e.* the elastic constants and their pressure dependence, the anisotropy factor, bulk modulus, shear modulus, Young's modulus, Lame's coefficient and Poisson's ratio. By means of the average sound velocity, the Debye temperature is evaluated for the CZTX studied solar materials. We have also calculated the thermal conductivity of these materials. The end of the chapter is reserved to exhibit the calculated thermodynamic properties *i.e.* thermodynamic functions and heat capacity of CZTX concerned crystals as functions of temperature in the range 0-1000 K.

III.2. Structural properties of CZTX solar materials

III.2.1. Study at zero pressure

Both types of the studied Cooper-based chalcogenides CZTX solar materials in this work are illustrated in Fig.3.1.

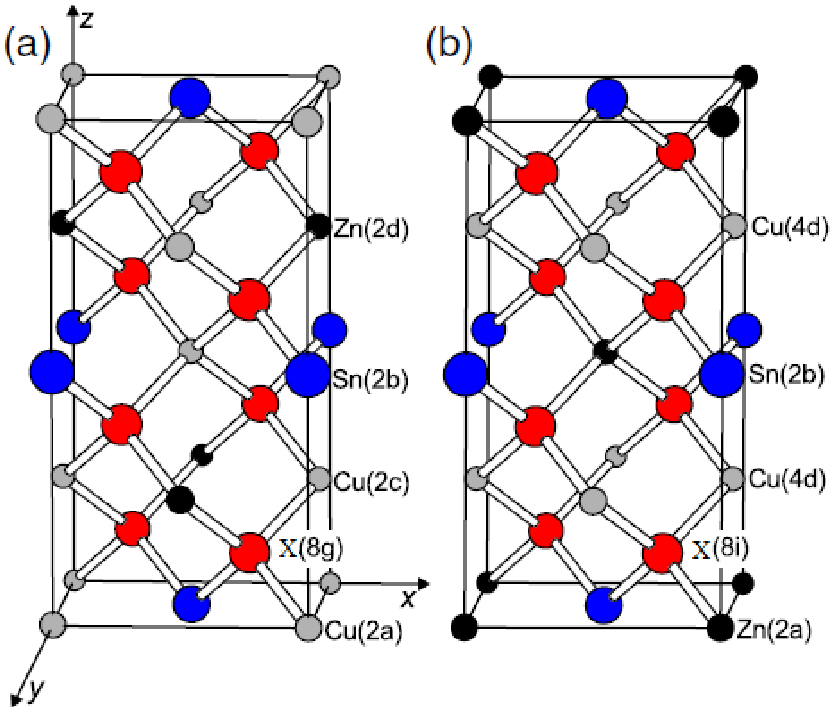

Fig.3.1: *Crystalline structure of (a) kesterite and (b) stannite conventional cells of CZTX solar materials.*

The kesterite CZTX with space group ($I\bar{4}$; no. 82) has in its conventional unit cell four Cu atoms on the Wyckoff positions 2*a* and 2*c*, two Zn atoms on position 2*d*, two Sn atoms on position 2*b*, and eight X atoms on the 8*g* position. The anion 8*g* position is defined by (*x*, *y*, *z*). The stannite structure with space group ($I\bar{4}2m$; no. 121) has four equivalent Cu atoms on Wyckoff 4*d* position, two Zn atoms on 2*a*, two Sn atoms on 2*b* and eight X atoms on the 8*i* position is defined by (*x*, *x* , *z*).

To construct graphical models of crystals we use the *materials visualizer module*, which is implanted in *Materials Studio* program commercialized by "Accelrys Software Inc." (Fig.3.2).

We relaxed the atomic positions; this relaxation lowered the total energy. The final structure obtained within GGA-WC approximation corresponds to the theoretical calculated structure.

The calculated lattice constants for the CZTX studied solar materials are listed in Table 3.1, the obtained results are in good agreement with the experimental reported structure data. The *c/a* ratio, which characterizes the tetragonal structure, is also estimated.

Table 3.1

Calculated lattice parameters (*a* and *c* in Å) and *c/a* ratio compared with experimental data.

	Present work [1]	Experiment	Theoretical
KS-CZTS			
a	5.393	5.427[a]	5.326[e]
c	10.797	10.871[a]	10.663[e]
c/a	2.002	-	-
ST-CZTS			
a	5.395	5.427[b]	5.325[e]
c	10.784	10.848[b]	10.629[e]
c/a	1.999	-	-
KS-CZTSe			
a	5.642	5.692[c]	5.605[e]
c	11.303	11.340[c]	11.200[e]
c/a	2.00	1.99[c]	-
ST-CZTSe			
a	5.650	5.688[d]	5.604[e]
c	11.270	11.338[d]	10.208[e]
c/a	1.995	1.993	-

[a] Reference [2], [b] Reference [3], [c] Reference [4], [d] Reference [5], [e] Reference [6].

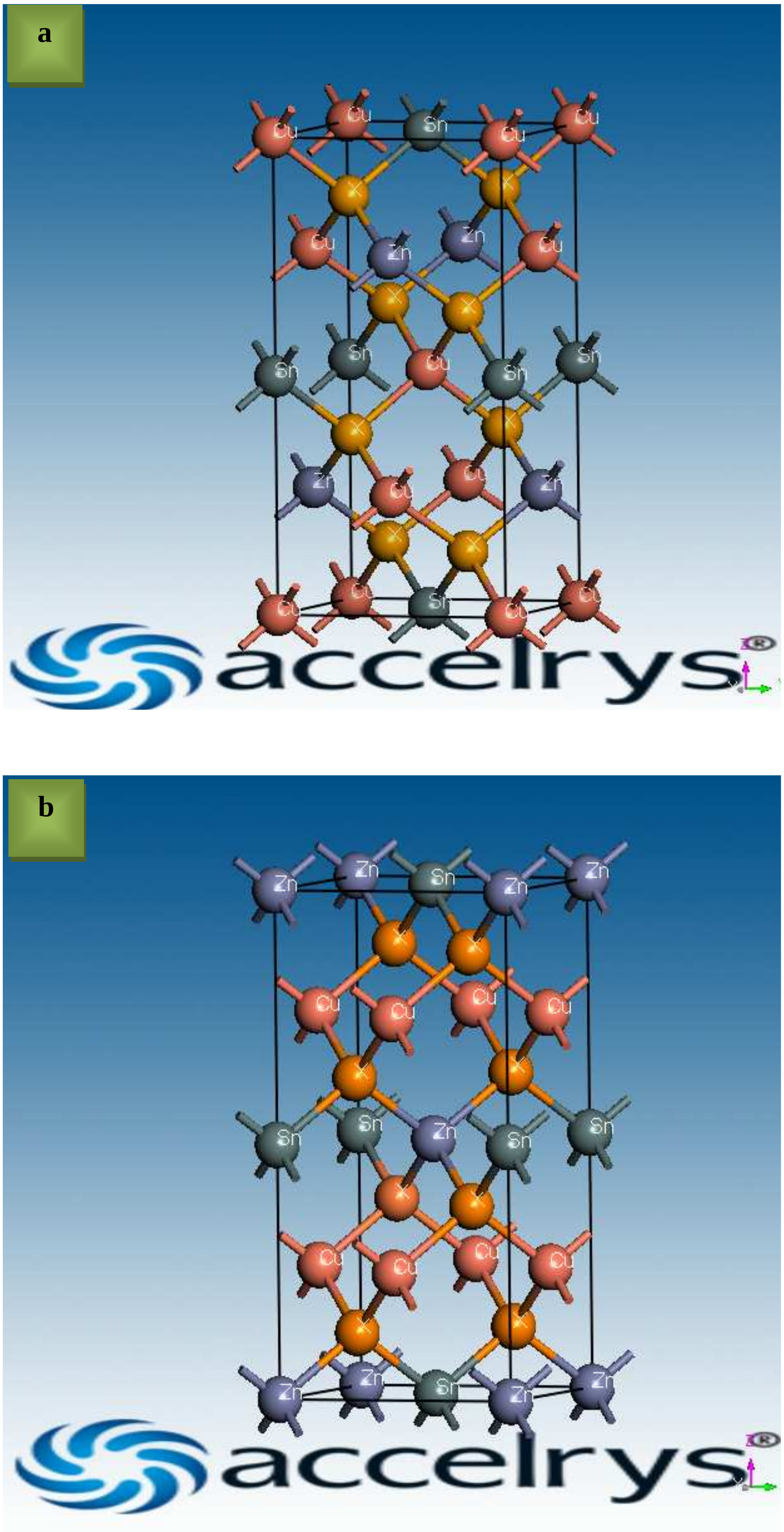

Fig.3.2: *Schematic illustration of (a):KS-CZTX and (b):ST-CZTX solar materials conventional cell obtained by materials visualizer module implanted in Materials Studio software program.*

The deviations between the experimental and the calculated conventional cell parameters *a* and *c* are estimated by less than 1 %. These deviations show that the present calculations are highly reliable.

From the calculated total energy difference, $E_t = E_{t(ST)} - E_{t(KS)}$ the most stable phase is the kesterite structure for both S-based and Se-based compounds. However, the total energy of the kesterite S-based compounds is only 2.4 meV/atom (1.3 meV/atom [6]) lower than the corresponding stannite structure.

Similarly, the total energy of the kesterite Se-based compounds is 2.5 meV/atom (3.3 meV/atom [6]) lower than their stannite structure. This indicates that kesterite and stannite are very similar and both phases may exist, furthermore, this similarity indicates, also, that KS and ST ordering may coexist in the synthesized samples.

III.2.2. Study under pressure effect (equation of state construction)

Employing calculated unit cell volumes (*V*) at fixed values of applied hydrostatic pressure (*P*) in the range 0-12 GPa, we construct the Birch-Murnaghan equation of state (EOS) [7]:

$$P = \frac{3}{2} B_0 \left[\left(\frac{V_0}{V} \right)^{\frac{7}{3}} - \left(\frac{V_0}{V} \right)^{\frac{5}{3}} \right] \times \left[1 + \frac{3}{4} \left(4 - B' \right) \left\{ \left(\frac{V_0}{V} \right)^{\frac{2}{3}} - 1 \right\} \right] \tag{III.1}$$

Here V_0 is fixed at the value determined from the zero pressure. The bulk modulus B_0 at zero pressure and its pressure derivative B' are evaluated as fitting parameters (Fig.3.3) and these are listed in Table 3.2.

Table 3.2

Evaluated B_0 (in GPa) and B' (dimensionless) from the Birch-Murnaghan EOS fitting [1].

	Sulphide compound		**Selenide compound**	
	KS-CZTS	ST-CZTS	KS-CZTSe	ST-CZTSe
B_0	78.4394	79.8789	67.6622	65.7059
B'	3.0913	3.3983	3.2197	2.7412

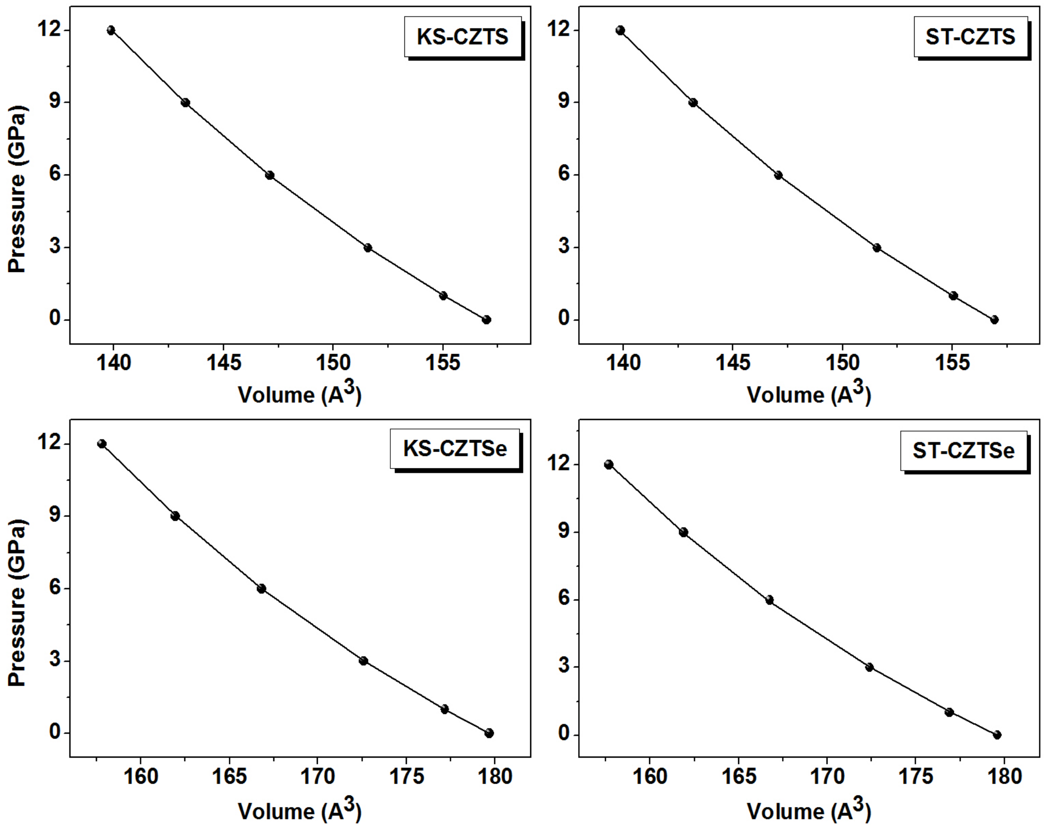

Fig.3.3: *The calculated pressure-volume relation for CZTX compounds. The symbols are the calculated results and the solid lines are given by the Birch-Murnaghan equation of state with the fitting parameters listed in Table 3.2* [1].

III.3. Elastic properties of CZTX solar materials

III.3.1. Elastic constants

III.3.1.1. Study at zero pressure

Elastic constants of CZTX compounds are listed in Table 3.3. The errors quoted for C_{ij} values are associated with the deviation of the stress strain relationship from linearity [8]. All elastic constants for both types of CZTX compounds are positive and satisfy the criteria [9] for mechanically stable crystals:

$$\left.\begin{array}{l} C_{11}>0, C_{33}>0, C_{44}>0, C_{66}>0, \\ (C_{11}-C_{12})>0, (C_{11}+C_{33}-2C_{13})>0, \\ \{2(C_{11}+C_{12})+C_{33}+4C_{13}\}>0 \end{array}\right\} \quad \text{(III.2)}$$

The calculated elastic constants of KS-CZTS and ST-CZTS have practically the same magnitude; accordingly, both types of the sulphide compound are indistinguishable mechanically. However, the calculated elastic constants of KS-CZTSe type are slightly greater compared to the calculated values of the ST-CZTSe type. It is noticed that the calculated elastic constants of sulphide compound are greater compared to the calculated values of the selenide compound for both considered types in this study.

Table 3.3

Calculated six independent elastic constants (C_{ij}) for CZTX solar materials (in GPa) [1].

	Sulphide compound		**Selenide compound**	
	KS-CZTS	ST-CZTS	KS-CZTSe	ST-CZTSe
C_{11}	105.582±0.804	104.190± 0.628	90.721 ± 0.477	87.599 ± 0.798
C_{33}	103.244 ±0.894	102.982± 0.627	90.274 ± 0.201	78.095 ± 10.325
C_{44}	49.778 ±2.171	50.252± 3.813	42.713 ± 0.783	38.924 ± 1.150
C_{66}	50.101±1.458	49.324 ± 1.519	41.730 ± 1.273	43.900 ± 6.048
C_{12}	67.343±0.891	68.764± 0.766	57.352 ± 0.384	57.102 ± 0.407
C_{13}	67.528±0.725	66.748± 0.600	57.174 ± 0.127	54.766 ± 1.344

III.3.1.2. Study under pressure effect

We present also the variation of the elastic constants of the considered types of CZTX compounds with respect to the variation of pressure in Fig.3.4. The solid curves are the second-order polynomial fit of the GGA-WC calculated data points. The values of pressure coefficients for the KS and ST type of the sulphide and selenide compounds are given in Table 3.4.

Table 3.4

Pressure coefficients of the calculated elastic constants: $C_{ij}(P)=C_{ij0}+\alpha P+\beta P^2$. C_{ij0} denotes the value of elastic constant at zero pressure [1].

	Sulphide compound				**Selenide compound**			
	KS-CZTS		ST-CZTS		KS-CZTSe		ST-CZTSe	
	α	β (GPa^{-1})	α	β (GPa^{-1})	α	β (GPa^{-1})	α	β (GPa^{-1})
C_{11}	4.3214	-0.0266	4.7435	-0.0607	4.2040	-0.0246	5.4048	-0.0950
C_{33}	4.3876	-0.0318	4.5922	-0.0499	4.0230	-0.0174	6.7453	-0.1703
C_{44}	0.1722	0.0001	-0.1621	-0.0169	-0.3275	0.0033	0.2038	-0.0023
C_{66}	0.1658	0.0038	0.2442	0.0038	-0.1458	-0.0330	0.6451	-0.0174
C_{12}	4.7152	-0.0244	5.3448	-0.0717	5.0995	-0.0360	5.4824	-0.0774
C_{13}	4.8852	-0.0180	5.1186	-0.0595	4.8753	-0.0284	5.7257	-0.1033

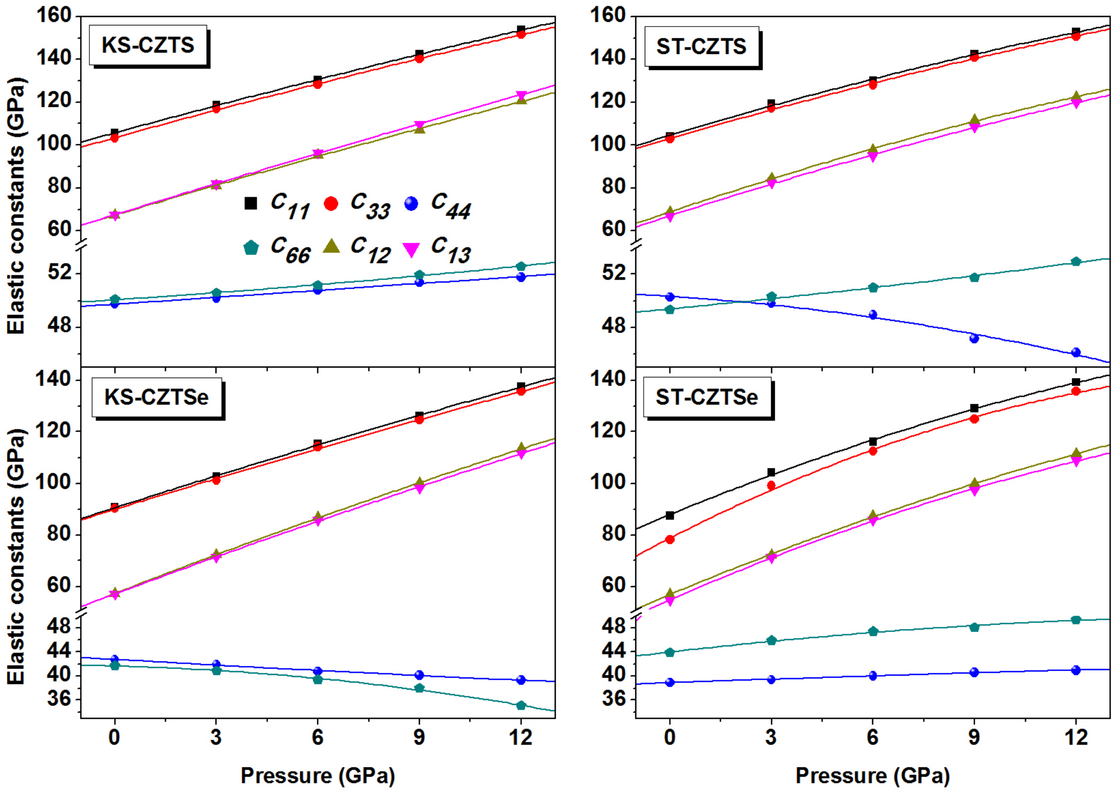

Fig.3.4: *Pressure effect on the calculated elastic constants for CZTX compounds. The solid lines are the second-order polynomial fit of the calculated data points* [1].

III.3.2. Anisotropy factor (A), bulk modulus (B) and shear modulus (G)

III.3.2.1. Study at zero pressure

We have also evaluated the anisotropy factor *A* for both considered types of our compounds; the shear anisotropic factor for the (001) shear plane between [110] and [010] directions is defined in the case of tetragonal symmetry by the following expression [9]:

$$A = \frac{2C_{66}}{C_{11} - C_{12}} \tag{III.3}$$

From Table 3.5, the computed values of *A* indicate that the elastic anisotropy for {001} shear planes between <110> and <010> directions for the ST-CZTX is somehow higher than KS type of CZTX materials.

In order to calculate the values of bulk modulus (*B*) and shear modulus (*G*) for polycrystalline materials two main approximations are used; the Voigt and Reuss schemes [11].

Table 3.5

Calculated anisotropy factor (*A*) and polycrystalline elastic moduli: bulk modulus (*B*) and shear modulus (*G*) for the KS and ST structure type of CZTS and CZTSe materials (B and G in GPa, A is dimensionless). The reported numbers within brackets refer to the theoretical data taken from references [9] and [10] for the sulphide and selenide compound respectively [1].

	Sulphide compound		**Selenide compound**	
	KS-CZTS	ST-CZTS	KS-CZTSe	ST-CZTSe
A	2.620±0.192 [2.28]	2.785±0.195	2.501±0.141 [2.30]	2.879±0.510
B_V	79.9118	79.5422	68.3462	65.1733
B_R	79.9024	79.5215	68.3453	64.7926
B_{VRH}	79.9070	79.5318	68.3458	64.9830
G_V	37.3989	37.2393	32.0989	30.1269
G_R	29.8788	29.3861	26.2064	23.4196
G_{VRH}	33.6388	33.3127	29.1527	26.7733

The Voigt approximation is the upper limit of the above-mentioned moduli, in the case of tetragonal symmetry, they are given by [12]:

$$\begin{cases} B_V = \frac{1}{9}\left[2\left(C_{11}+C_{12}\right)+C_{33}+4C_{13}\right] \\ G_V = \frac{1}{30}\left[M+3C_{11}-3C_{12}+12C_{44}+6C_{66}\right] \\ M = C_{11}+C_{12}+2C_{33}-4C_{13} \end{cases} \tag{III.4}$$

While the Reuss approximation corresponds to the lower limit of these parameters, in the case of tetragonal symmetry, they are given by [12]:

$$\begin{cases} B_R = \frac{C^2}{M} \\ G_R = \frac{15}{\left\{\left[2\left(2\left(C_{11}+C_{12}\right)+C_{33}+4C_{13}\right)/C^2\right]+6/\left(C_{11}-C_{12}\right)+6/C_{44}+3/C_{66}\right\}} \\ C^2 = \left(C_{11}+C_{12}\right)C_{33}-2C_{13}^2 \end{cases} \tag{III.5}$$

Then, Hill ($B_{VRH} \equiv B$ and $G_{VRH} \equiv G$) takes the average:

$$B = \frac{B_V + B_R}{2} \tag{III.6}$$

$$G = \frac{G_V + G_R}{2} \qquad \text{(III.7)}$$

The values of the bulk modulus and the shear modulus of both structures of the sulphide compound are practically the same. However, the bulk modulus and the shear modulus of the KS type are slightly higher than those of the ST type of the selenide CZTSe.

From Table 3.2, the obtained values of bulk modulus from the EOS (78.4394 GPa and 79.8789 GPa for the KS and ST type respectively of the sulphide compound, 67.6622 GPa and 65.7059 GPa for the KS and ST type respectively of the selenide compound) are close to the calculated values from the single crystal elastic constants (79.9071 GPa and 79.5318 GPa for the KS and ST type respectively of the sulphide compound, 68.3458 GPa and 64.9830 GPa for the KS and ST type respectively of the selenide compound), which enhances the accuracy of present calculations.

III.3.2.2. Study under pressure effect

The effect of hydrostatic gradient pressure is studied in the considered herein range *i.e.* (0-12 GPa). The variation of the anisotropy factor with the applied pressure is illustrated in Fig.3.5; we observe a clear increasing of the anisotropy factor in the considered range pressure, and this for all CZTX compounds.

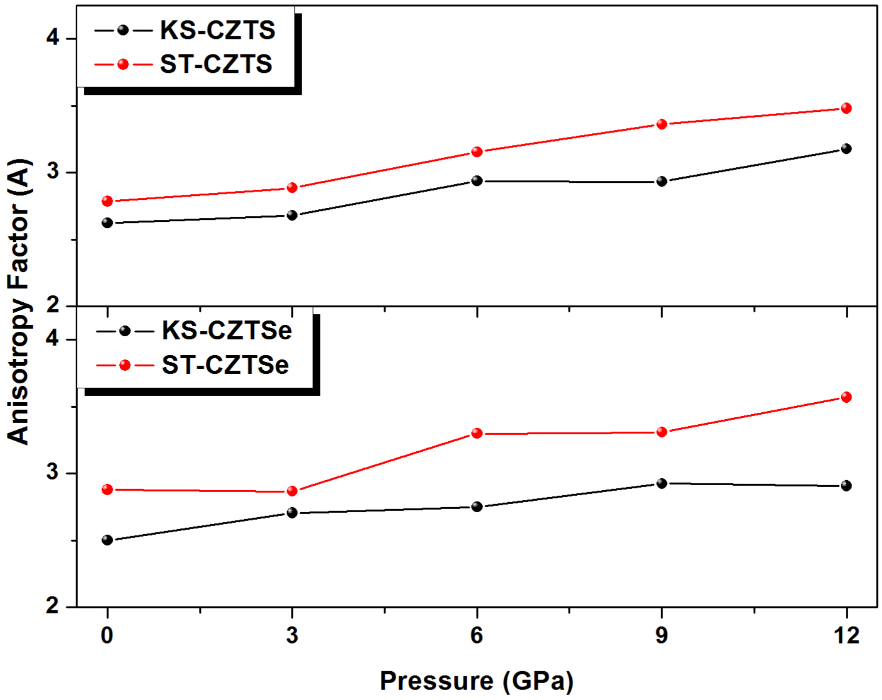

Fig.3.5: *Anisotropy factor-Pressure allures for CZTX solar materials.*

We also, studied the effect of the external hydrostatic pressure on the bulk modulus (B) and shear modulus (G) for CZTX concerned solar materials. The evolution of bulk and shear moduli is illustrated in Fig.3.6; the bulk modulus increases monotonically with pressure for all studied solar materials, however, the shear modulus show a few decreasing with respect to pressure gradient for KS-CZTS, ST-CZTS and KS-CZTSe, on the other hand, it exhibits a no monotonically behavior in the case of ST-CZTSe.

Inter alia, we performed a quadratic polynomial fit based on the calculated point; and this, in order to obtain the pressure coefficients from the following equations:

$$\begin{cases} B(P) = B_0 + \alpha P + \beta P^2 \\ G(P) = G_0 + \alpha P + \beta P^2 \end{cases} \tag{III.6}$$

Here; B_0 and G_0 denote, the value of bulk modulus (B) and shear modulus (G), respectively at zero pressure. The calculated pressure coefficients of the calculated bulk modulus (B) and shear modulus (G) are listed in Table 3.6 below.

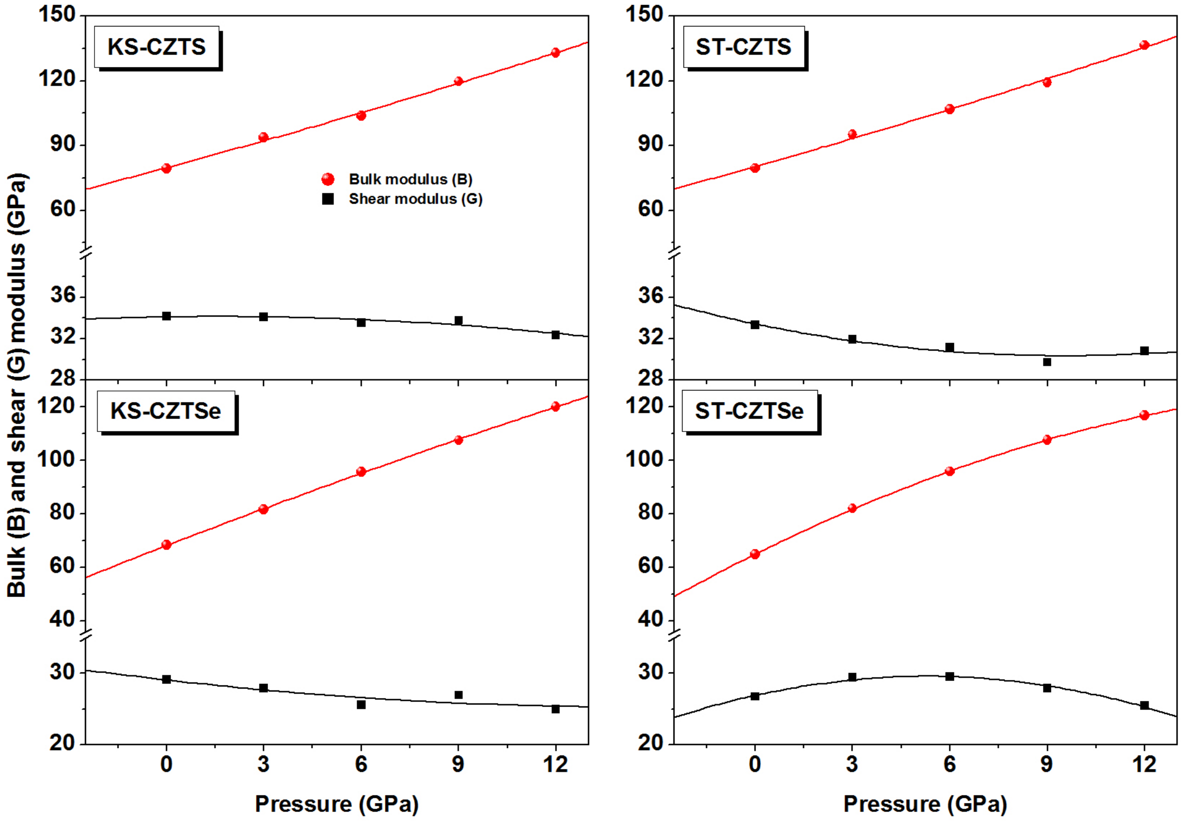

Fig.3.6: *Bulk modulus (B) and shear modulus (G) under pressure for CZTX solar materials. The solid lines are the quadratic fit of the calculated points.*

Table 3.6:

Pressure coefficients of the calculated bulk modulus (*B*) and shear modulus (*G*).

	Sulphide compound				**Selenide compound**			
	KS-CZTS		ST-CZTS		KS-CZTSe		ST-CZTSe	
	α	β (GPa^{-1})	α	β (GPa^{-1})	α	β (GPa^{-1})	α	β (GPa^{-1})
B	4,0607	0,0311	4,2274	0,0308	4,6841	-0,0309	6,0111	-0,1416
G	0,0464	-0,0148	-0,6506	0,0341	-0,5237	0,0178	1,0143	-0,0960

III.3.3. Young's modulus, Lame's coefficient and Poisson's ratio

III.3.3.1. Study at zero pressure

The Young's modulus (*E*), Lame's coefficient (λ) and Poisson's ratio (σ) are given by the following equations [13]:

$$E = \frac{9BG}{3B+G} \tag{III.8}$$

$$\lambda = \frac{E\sigma}{1-\sigma-2\sigma^2} \tag{III.9}$$

$$\sigma = \frac{3B-E}{6B} \tag{III.10}$$

Those parameters are evaluated at zero pressure; the obtained values are illustrated in Table 3.7. The isotropic Young modulus, which is defined by the ratio between stress and strain, is usually used to provide a measure of the stiffness of the solid.

Table 3.7

Calculated polycrystalline elastic moduli: Young's modulus (*E*), Lame's coefficient (λ) and Poisson's ratio (σ) for the KS and ST structure type of CZTS and CZTSe materials (*E* and λ in GPa, σ is dimensionless). The reported numbers within brackets refer to the theoretical data taken from references [9] and [10] for the sulphide and selenide compound respectively [1].

	Sulphide compound		**Selenide compound**	
	KS-CZTS	ST-CZTS	KS-CZTSe	ST-CZTSe
E	88.498	87.694	76.571	70.621
λ	57.295	57.221	48.806	47.181
σ	0.315 [0.308]	0.316	0.313 [0.310]	0.319

We found for the sulphide compound that $E_{(KS)} \approx E_{(ST)}$; suggesting that KS-CZTS and ST-CZTS have the same stiffness character. However, for the selenide compound; we found that, $E_{(KS)} > E_{(ST)}$; suggesting that KS-CZTSe type is more stiff than ST-CZTSe. Furthermore, the obtained results show that the sulphide compound is more stiff compared to the selenide compound.

II.3.2.2. Study under pressure effect

The graphical evolution of Poisson's ratio (σ) and those polycrystalline parameters is illustrated in Fig.3.7 and Fig.3.8, respectively. Furthermore, the calculated pressure derivatives of Young's modulus (E) and Lame's coefficient (λ) for CZTX solar materials are illustrated in Table 3.8.

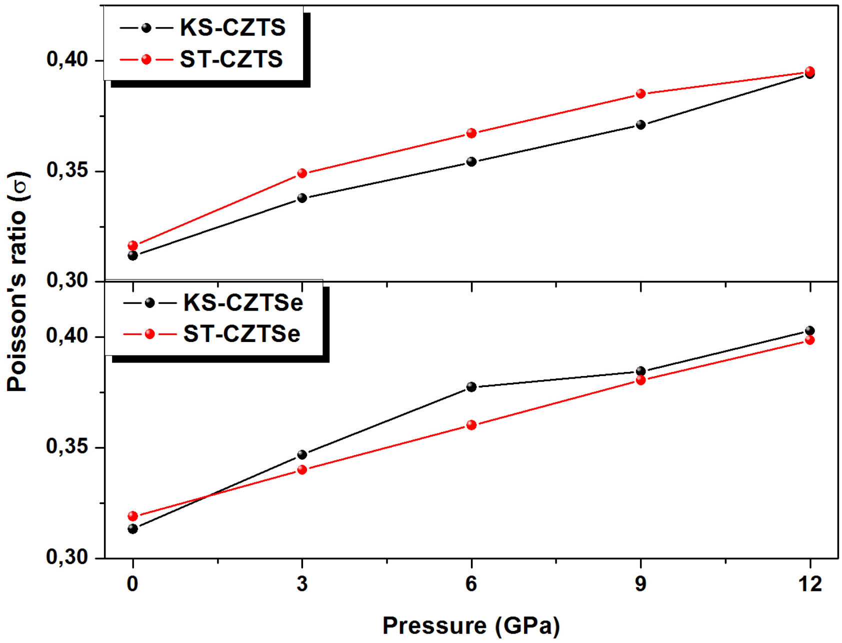

Fig.3.7: *Poisson's ratio-Pressure allures for CZTX solar materials.*

Table 3.8

Calculated pressure derivatives of Young's modulus (E) and Lame's coefficient (λ) for the KS and ST structure type of CZTS and CZTSe materials.

	Sulphide compound		**Selenide compound**	
	KS-CZTS	ST-CZTS	KS-CZTSe	ST-CZTSe
$\partial E/\partial P$	0.378	-0.511	-0.593	0.7602
$\partial \lambda/\partial P$	4.611	4.757	4.520	4.404

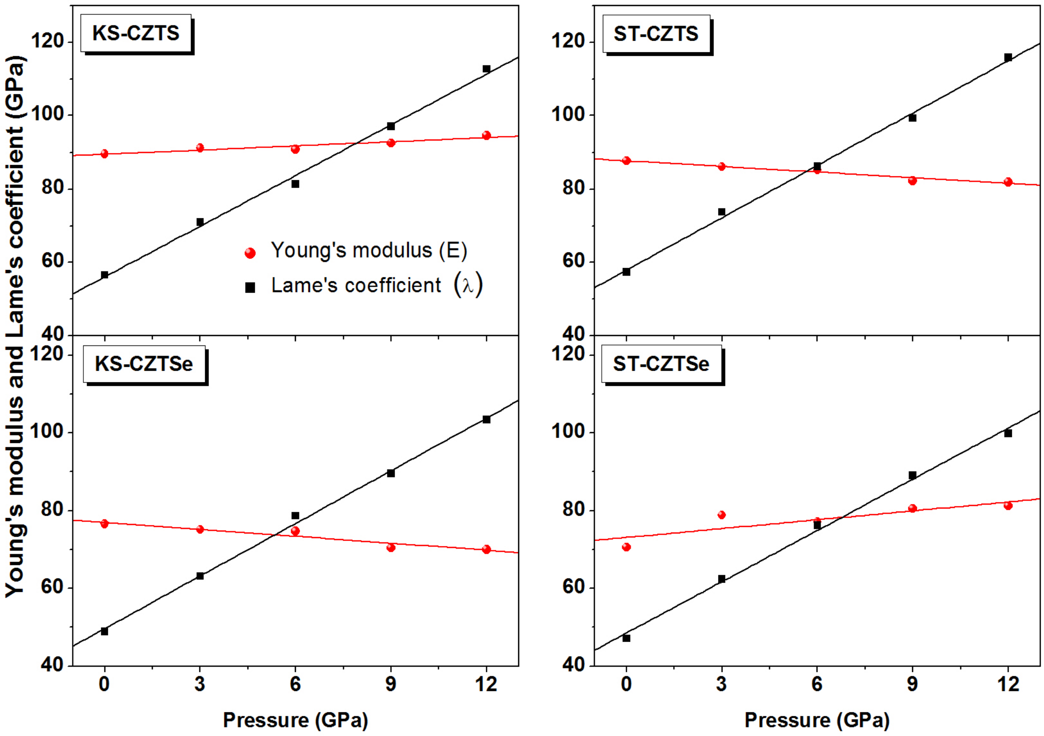

Fig.3.8: *Pressure dependence of Young's modulus (E) and Lame's coefficient (λ) for CZTX solar materials. The solid lines are the linear fit of the calculated points.*

III.3.4. Mechanical behavior prediction

According to Pugh's [14] empirical relationship; the *B/G* ratio can classify materials as ductile or brittle according to a critical value. If *B/G* ratio is greater than 1.75 the material behaves as ductile, otherwise the material behaves as brittle.

The table 3.9 illustrates the calculated results. The estimated numerical values of *B/G* ratio for the sulphide compound are 2.375 and 2.387 for KS and ST structure, respectively, classifying CZTS material as ductile. For the selenide compound; we found that *B/G* ratios are 2.344 and 2.427 for KS and ST structure, respectively, classifying CZTSe material as ductile, moreover; the ST type is more ductile than KS type for CZTX compounds especially in the case of the selenide compound.

We have also studied the evolution of *B/G* ration with hydrostatic pressure. In Fig.3.9 we show the *B/G-P* diagram, furthermore, the coefficients of the performed quadratic fit based on the GGA-WC calculated ratio is illustrated in Table 3.10.

Table 3.9

Deduced *B/G* ratio for the KS and ST structure type of CZTS and CZTSe materials. The reported numbers within brackets refer to the theoretical data taken from references [9] and [10] for the sulphide and selenide compound respectively [1].

	Sulphide compound		**Selenide compound**	
	KS-CZTS	ST-CZTS	KS-CZTSe	ST-CZTSe
B/G	2.375 [2.28]	2.387	2.344 [2.303]	2.427

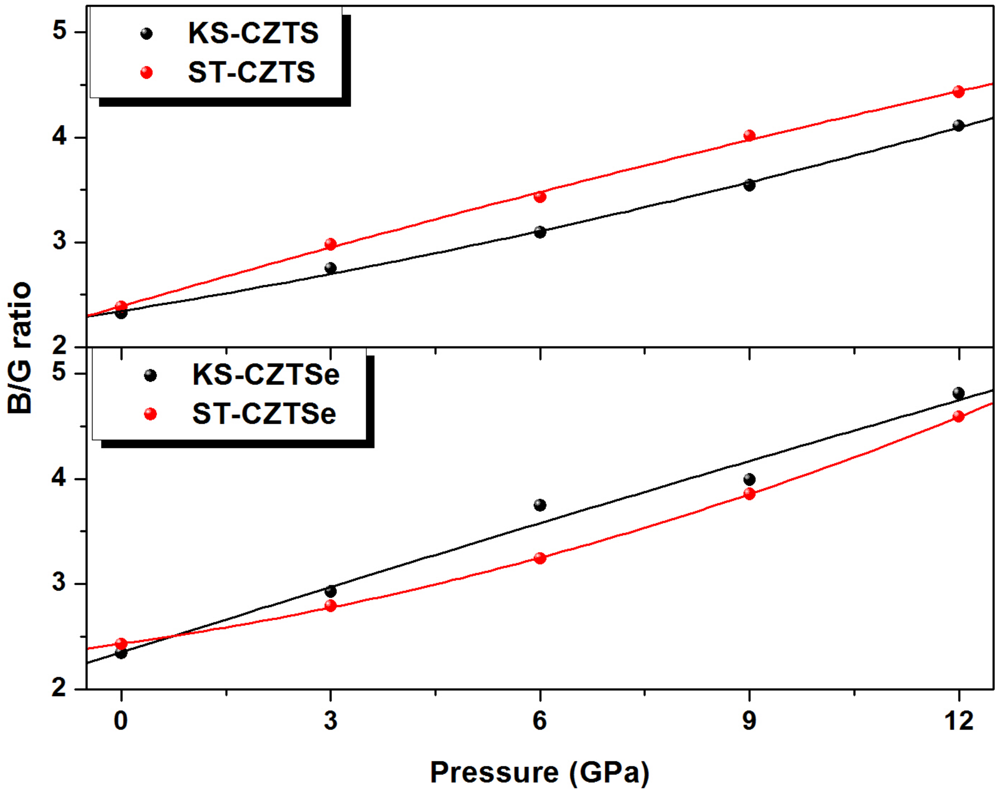

Fig.3.9: Pressure effect on the calculated *B/G* ratio for CZTX compounds. The solid lines are the second-order polynomial fit of the calculated data points.

Table 3.10

Pressure coefficients of the calculated *B/G* ratio. $B/G(P)= (B/G)_0+\alpha P+\beta P^2$. $(B/G)_0$ denotes the value of *B/G* ratio at zero pressure.

Sulphide compound				**Selenide compound**			
KS-CZTS		ST-CZTS		KS-CZTSe		ST-CZTSe	
α (GPa^{-1})	β (GPa^{-2})	α (GPa^{-1})	β (GPa^{-2})	α (GPa^{-1})	β (GPa^{-2})	α (GPa^{-1})	β (GPa^{-2})
0.1087	0.0031	0.1915	-0.0017	0.2092	-0.0008	0.0928	0.0072

III.3.5. Debye temperature of CZTX solar materials

III.3.5.1. Study at zero pressure

The Debye temperature is an important parameter in solids; it is linked to many physical properties such as specific heat, elastic constants, and melting temperature [15]. Using the average sound velocity (v_m), the Debye temperature (θ_D) can be deduced according to following equation [15]:

$$\theta_D = \frac{h}{k_B}\left[\frac{3n}{4\pi}\times\frac{N_A\rho}{M}\right]^{\frac{1}{3}}\times v_m \tag{III.11}$$

Where h is the Plank's constant, k_B is the Boltzmann's constant, N_A is the Avogadro's number, ρ is the density, M is the molecular weight and n is the number of atoms in the molecule. The average sound velocity (v_m) in polycrystalline materials is given by [15]:

$$v_m = \left[\frac{1}{3}\left(\frac{2}{v_t^3}+\frac{1}{v_l^3}\right)\right]^{-\frac{1}{3}} \tag{III.12}$$

Where v_t and v_l designate the transverse and longitudinal sound velocities and are given by Navier’s equation [15]:

$$v_t = \left(\frac{3B+4G}{3\rho}\right)^{\frac{1}{2}} \tag{III.13}$$

$$v_l = \left(\frac{G}{\rho}\right)^{\frac{1}{2}} \tag{III.14}$$

The calculated ρ, v_t, v_l, v_m and θ_D are given in Table 3.11. The obtained results predict that both types of CZTS have practically the same Debye temperature (θ_D), however, θ_D of KS-CZTSe is higher than that of ST-CZTSe. On the other hand, to the best of our knowledge, there are no data available in the literature on these properties for the considered types of herein studied CZTX compounds.

Table 3.11

Calculated density (ρ), transverse (v_t), longitudinal (v_l), average sound velocity (v_m) from the GGA-WC obtained polycrystalline elastic modulus and the Debye temperature (θ_D) for both CZTX compounds types considered in this study [1].

	$\rho(g/cm^3)$	v_t (m/s)	v_l (m/s)	v_m (m/s)	θ_D (K)
Sulphide					
KS-CZTS	4.6484	5181	2690	3573	394
ST-CZTS	4.6494	5163	2677	3557	393
Selenide					
KS-CZTSe	5.7871	4304	2244	2979	314
ST-CZTSe	5.7882	4171	2151	2861	302

III.3.5.2. Study under pressure effect

We have also studied the effect of hydrostatic pressure on the calculated density, (ρ), the transverse, (v_t), the longitudinal, (v_l), and the average sound velocity, (v_m). The obtained allures are shown in Fig.3.10 and Fig.3.11 bellow. However, in Tables 3.12 and 3.13, we illustrate the coefficients of the performed fits based on the calculated GGA-WC points.

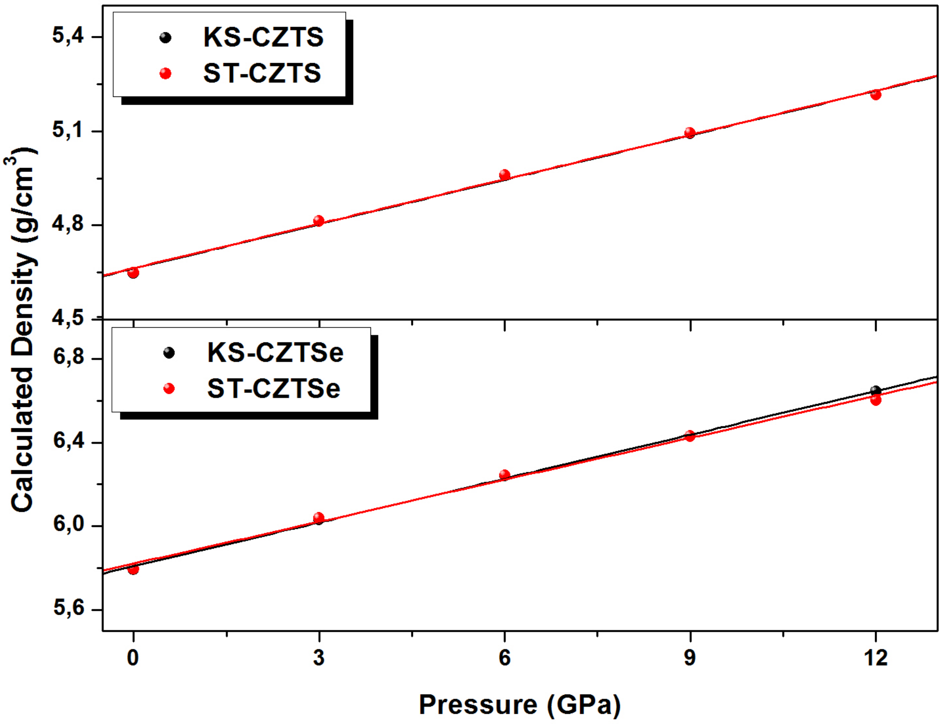

Fig.3.10: Pressure effect on the calculated density for CZTX compounds. The solid lines are the linear fit of the calculated data points.

Form Fig.3.10, we observe that, the calculated density for CZTX materials have identical allures as function of external applied hydrostatic pressure concerning the studied types; especially in the case of S-based compound, however, the ST and KS allures of calculated density-pressure are somehow different at high pressure in the case of Se-based compound. Generally, both types of CZTX compounds have rather similar pressure derivatives in the herein pressure range as shown in Table 3.12.

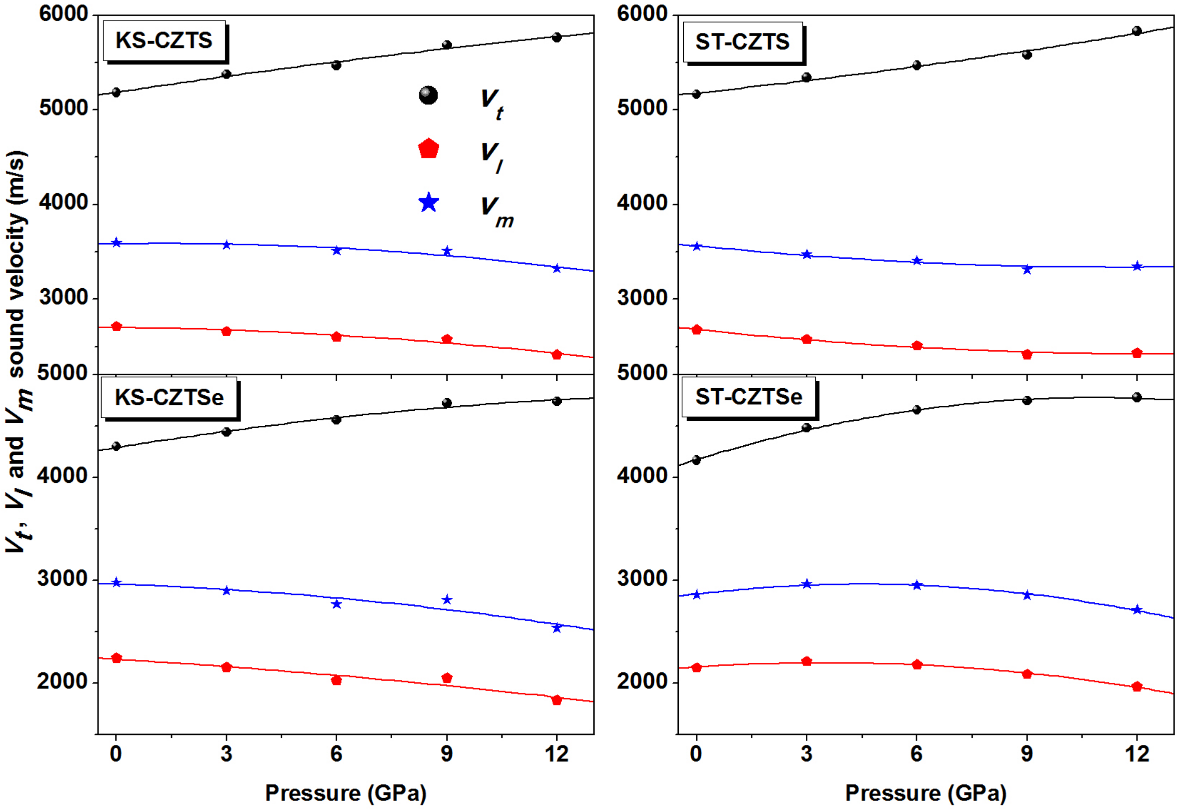

Fig.3.11: Pressure effect on the calculated transverse (v_t), longitudinal (v_l) and average sound velocity (v_m) density for CZTX compounds. The solid lines are the quadratic fit of the calculated data points.

From Fig.3.11, the characteristic sound velocities for our considered compounds exhibit a quadratic behavior versus applied hydrostatic pressure. The coefficients of the performed quadratic fit from the calculated GGA-WC data points are shown in Table 3.13 below.

Table 3.12

Evaluated pressure derivative of calculated density (ρ) for the KS and ST structure type of CZTS and CZTSe materials ($g/cm^3/GPa$).

	Sulphide compound		**Selenide compound**	
	KS-CZTS	ST-CZTS	KS-CZTSe	ST-CZTSe
$\partial\rho/\partial P$	0.0472	0.0471	0.0698	0.0668

Table 3.13

Pressure coefficients of the calculated: transverse (v_t), longitudinal (v_l) and average sound velocity (v_m). $v(P)= v_0+\alpha P+\beta P^2$. v_0 denotes the value of the concerned velocity at zero pressure (α in $ms^{-1}GPa^{-1}$ and β in $ms^{-1}GPa^{-2}$).

	Sulphide compound				**Selenide compound**			
	KS-CZTS		ST-CZTS		KS-CZTSe		ST-CZTSe	
	α	β	α	β	α	β	α	β
v_t	58.7362	-0.8064	-39.3143	1.6873	58.2181	-1.6254	111.2962	-5.1397
v_l	-4.8062	-1.4992	40.7752	0.9810	-21.6033	-0.7722	23.5581	-3.3365
v_m	5.3133	-2.1222	-41.9833	1.6833	-11.8729	-1.7103	41.5410	-4.5873

III.3.6. Thermal conductivity of CZTX solar materials

The thermal conductivity of CZTX solar alloys were evaluated using two theoretical methods: Clarke's [16] and Cahill's [17] model. The formulas are given by:

$$\kappa_{min} = 0.87 K_B \bar{M}^{-2/3} E^{1/2} \rho^{1/6} \qquad \text{(III.15)}$$

$$\kappa_{min} = \frac{K_B}{2.48} p^{2/3} \left(v_l + 2v_t \right) \qquad \text{(III.16)}$$

Here: $\bar{M} = \frac{M}{nN_A}$; is the average mass per atom, n the number of atoms per unit cell, p the density of number of atoms per volume. The calculated minimum thermal conductivities are listed in Table 3.14.

Table 3.14

Minimum thermal conductivity calculated through Clark and Cahill models for both CZTX compounds types considered in this study.

Compound	**Sulphide compound**				**Selenide compound**			
Type	KS-CZTS		ST-CZTS		KS-CZTSe		ST-CZTSe	
Model	Clark	Cahill	Clark	Cahill	Clark	Cahill	Clark	Cahill
κ_{min} (W/mK)	0.7204	0.9988	0.7172	0.9952	0.5485	0.7585	0.5268	0.7334

III.4. Thermodynamic properties of CZTX crystals

Using phonon calculations in CASTEP code, we can evaluate the temperature dependence of the energy, entropy, free energy and lattice heat capacity of a crystal in the framework of quasi-harmonic approximation.

III.4.1. Background theory of thermodynamic calculations in CASTEP

The vibrational contributions to the thermodynamic properties are evaluated to compute the internal energy (*U*), the free energy (*F*), the entropy (*S*) and heat capacity (C_v) at finite temperatures.

Based on the work of Baroni et al [18], which focuses on the phonons and related crystal properties from density-functional perturbation theory, the formulas of vibrational contributions to the mentioned thermodynamic properties are provided below.

The phonon contribution to the internal energy is given by:

$$U = \int \frac{\hbar\omega}{exp\left(\frac{\hbar\omega}{kT}\right)} F(\omega) d\omega \tag{III.17}$$

Here; *k* is Boltzmann's constant, *ħ* is Planck's reduced constant and *F(ω)* is the phonon density of states.

The vibrational contribution to the free energy (*F*) is given by:

$$F = kT \int F(\omega) ln\left[1 - exp\left(-\frac{\hbar\omega}{kT}\right)\right] d\omega \tag{III.18}$$

The vibrational contribution to the entropy (*S*) can be calculated using the following relation:

$$S = k\left\{ \int \frac{\frac{\hbar\omega}{kT}}{exp\left(\frac{\hbar\omega}{kT}\right)-1} F(\omega)d\omega - \int F(\omega)\left[1-exp\left(-\frac{\hbar\omega}{kT}\right)\right]d\omega \right\} \tag{III.19}$$

The lattice contribution to the heat capacity (C_v) is:

$$C_v = k\int \frac{\left(\frac{\hbar\omega}{kT}\right)^2 exp\left(\frac{\hbar\omega}{kT}\right)}{\left[exp\left(\frac{\hbar\omega}{kT}\right)-1\right]^2} F(\omega)d\omega \tag{III.20}$$

III.4.2. Thermodynamic functions of CZTX crystals

In this work, the thermodynamic properties are calculated in the temperature range from 0 to 1000 K for the considered types of the studied compounds. The entropy (*S*), the free energy (*F*) and the internal energy (*U*) of CZTX crystals are illustrated in Figs. 3.12, 3.13 and 3.14 respectively.

III.4.2.1. Entropy of CZTX crystals under thermal gradient

The calculated entropy (see Fig.3.12) increases with temperature gradient for both compounds, besides; *S* is less sensitive to the temperature gradient in the case of the ST structure compared to KS structure for both CZTX compounds. It is noticed that, the ST and KS entropy-temperature curves are more identical in the case of sulphide compound compared to selenide compound.

III.4.2.2. Free energy of CZTX crystals under thermal gradient

The Fig.3.13 illustrates that, the free energy (*F*) decreases algebraically with increasing temperature for both compounds for both types. The KS type is somehow more sensitive to temperature increasing; especially at high temperature. In addition, the ST and KS free energy-temperature curves are more identical in the case of sulphide compound compared to selenide compound.

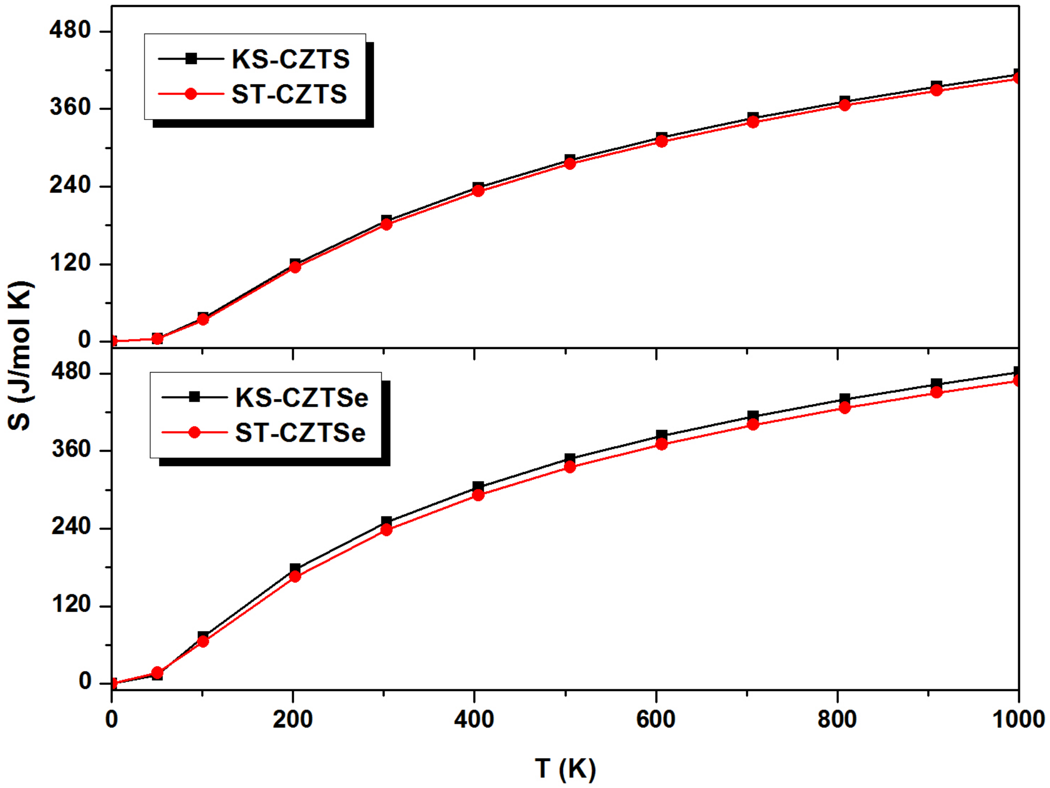

Fig.3.12: Calculated entropy vs. T for CZTX compounds [1].

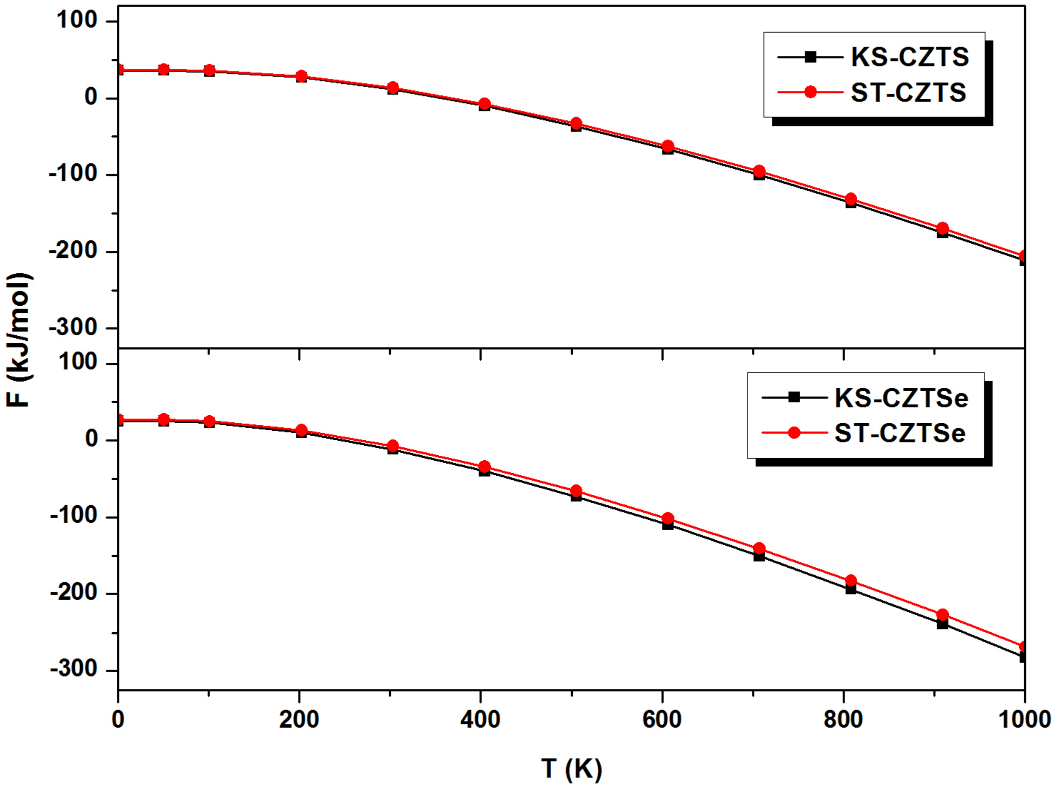

Fig.3.13: Calculated free energy vs. T for CZTX compounds [1].

III.4.2.3. Internal energy of CZTX crystals under thermal gradient

As Fig.3.14 shows; the internal energy (*U*) increases under thermal gradient for both alloys, we note also that, *U* is almost insensitive to the type of CZTX crystals; where KS and ST internal energy-temperature graphs are identical for the sulphide and selenide compounds.

The zero point energy presents the value of the free energy and the internal energy at zero temperature. It is 35.95 kJ/mol and 36.95 kJ/mol for KS and ST type; respectively for the sulphide compound, and it is 25.47 kJ/mol and 27.16 kJ/mol for KS and ST type; respectively for the selenide compound. However, to the best of our knowledge, there are no available values of this parameter for the CZTX crystals. Therefore, our calculations could be taken as predictions.

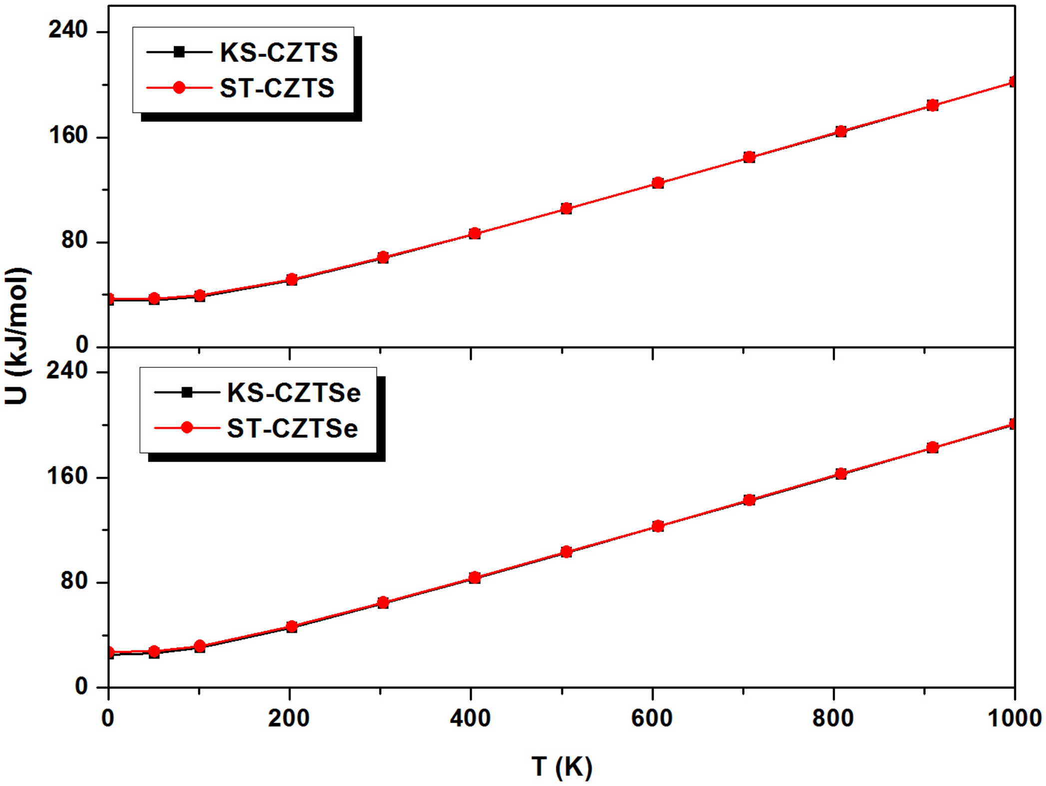

Fig.3.14: Calculated internal energy vs. T for CZTX compounds [1].

III.4.3. Heat capacity of CZTX crystals

The calculated heat capacity shows that the variation with temperature of C_v of both studied solar materials for the considered types exhibits similar features (Fig.3.15).

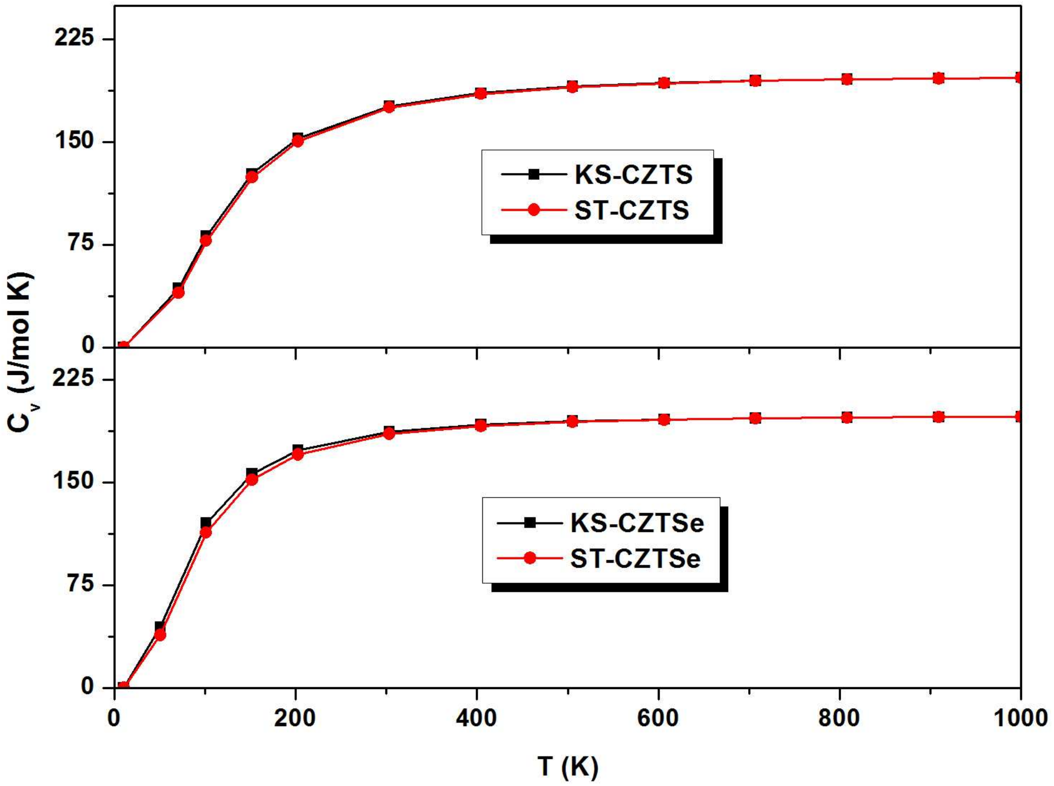

Fig.3.15: Calculated heat capacity vs. T for CZTX compounds [1].

Increasing temperature leads to a rapidly increasing of C_v at lower temperature, then a slow increasing at high temperature and converges to a constant value. It is clear that when T<500 K; C_v is proportional to T^3 [19], however; at high temperature region it tends to the Petit and Dulong limit [20] which is around 198 J/mol K for both types of the considered CZTX solar alloys.

III.5. Summary

In this last chapter, we have presented and discussed our foremost-obtained results. First of all, we have approached the structural parameters of CZTX solar materials at zero pressure and under hydrostatic applied pressure. Then we dealt with about elastic properties, where we exposed the calculated elastic constants, their behavior under pressure gradient, the mechanical behavior of these solar alloys is predicted as ductile. In the framework of quasi-harmonic Debye model and by the use of finite displacement method implanted in CASTEP software program we have evaluated the thermal behavior of some thermodynamic properties of CZTX solar materials *i.e.* the internal energy, the entropy, the free energy, and heat capacity C_v which is obtained around of "198 J/mol K" at high temperature range for all the studied compounds.

References

[1] S. Bensalem, M. Chegaar, D. Maouche, A. Bouhemadou, J. Alloys. Compd. 589 (2014) 137.

[2] S. R. Hall, J. T. Szymanski, J. M. Stewart, Can. Mineral. 16 (1978) 131.

[3] W. Schafer, R. Nitsche, Mat. Res. Bull. 9 (1974) 645.

[4] T. Maeda, S. Nakamura, T. Wada, Thin Solid Films 519 (2011) 7513.

[5] I. D. Olekseyuk, L. D. Gulay, I. V. Dydchak, L. V. Piskach, O. V. Parasyuk, O. V. Marchuk, J. Alloys. Compd. 340 (2002) 141.

[6] C. Persson, J. Appl. Phys. 107 (2010) 053710.

[7] F. Birch, J. Geophys. Res. 83 (1978) 1257.

[8] A. A. Gusev, M. M. Zehnder, U. W. Suter, Phys. Rev. B 54 (1996) 1.

[9] X. He, H. Shen, Physica B 406 (2011) 4604.

[10] X. He, H. Shen, Phys. Scripta. 85 (2012) 035302.

[11] J. F. Nye, Propriétés physiques des cristaux, Dunod, Paris, 1961.

[12] H. Zhai1, X. Li, J. Du, Mater. Trans. 53 (2012) 1247.

[13] E. Schreiber, O. L. Anderson, N. Soga, *Elastic constants and their measurement,* McGraw-Hill, New York, 1973.

[14] S. F. Pugh, Philos. Mag. 45 (1954) 823.

[15] O. L. Anderson, J. Phys. Chem. Solids 24 (1963) 909.

[16] D. R. Clarke, Surf. Coat. Technol. 163 (2003) 67.

[17] D. G. Cahill, S. K. Watson, R. O. Pohl, Phys. Rev. B 46 (1992) 6131.

[18] S. Baroni, S. de Gironcoli, A. dal Corso, P. Giannozzi, Rev. Mod. Phys. 73 (2001) 515.

[19] P. Debye, Ann. d. Phys. 39 (1912) 789.

[20] A. T. Petit, P. L. Dulong, Ann. Chim. Phys. 10 (1819) 395.

Conclusion

CONCLUSION

The search for sustainable energy sources and a solution to the environmental impacts of fossil energies exploitation dilemma have become the greatest concerns regarding our future. Economic and environmental constraints are pushing us to change how we harness and utilize vital energy, and these constraints will increase over the next few decades with the growing world demand for energy.

A useful method to contribute to the sustainable generation movement and environment protection is the use of photovoltaic generators to convert solar energy into electricity.

Solar cells are devices that use solar radiation to generate electricity; the field of photovoltaic solar materials has recently received more attention as efforts are being made to improve solar materials competitiveness. However, for photovoltaic devices to reach their full potential, novel materials need to be developed to allow higher performance, reasonable cost and clean based chemical species.

In this thesis, four solar materials have been studied through a theoretical approach, they are: kesterite Cu_2ZnSnS_4, stannite Cu_2ZnSnS_4, kesterite $Cu_2ZnSnSe_4$ and stannite $Cu_2ZnSnSe_4$, which are abbreviated CZTX in this work. Our contribution focused on the investigation of fundamental physical properties of these new attractive solar materials for photovoltaic energy application.

We have studied the structural, elastic and thermodynamic properties of the four compounds employing first principles approach, using the plane wave pseudo potential calculations (PP-PW) implemented in the CASTEP package within Density Functional Theory (DFT) and the Generalized Gradient Approximation of Wu-Cohen (GGA-WC).

The obtained results show that; the calculated lattice parameters are in good agreement with experimental reported data. The deviations between the experimental and the calculated conventional cell parameters a and c are estimated by less than 1 %. These deviations show that the present calculations are highly reliable. From the calculated total energy difference, the most stable phase is the kesterite structure for both S-based and Se-based compounds.

The elastic constants are calculated for both types of both compounds using the static finite strain scheme; the pressure dependence of elastic constants is predicted. The bulk modulus, anisotropy factor, shear modulus, Young's modulus, Lame's coefficient and Poisson's ratio have been estimated from the calculated single crystalline elastic constants.

The computed values of the anisotropy factor (*A*) indicate that the elastic anisotropy for {001} shear planes between <110> and <010> directions for the ST-CZTX is somehow higher than KS type of CZTX materials.

The values of the bulk modulus and the shear modulus of both structures of the sulphide compound are practically the same. However, the bulk modulus and the shear modulus of the KS type are slightly higher than those of the ST type of the selenide CZTSe.

A good correlation has been established between the calculated values of bulk modulus (*B*) from the EOS, and those calculated from the single crystal elastic constants; this enhances the accuracy of the performed calculations.

Based on the Pugh's empirical relationship; the calculated *B/G* ratios for the studied materials are greater than 1.75 which is the critical distinctive value between the ductile and the brittle behavior. Accordingly, CZTX compounds behave as ductile.

The Debye temperature is deduced using the average sound velocity, in fact, the density (ρ), transverse (v_t), longitudinal (v_l) and average sound velocity (v_m) are evaluated for the studied alloys considering both KS and ST types structures. Furthermore, the thermal conductivity of CZTX solar materials was evaluated using two theoretical methods: Clarke’s and Cahill’s model.

We have also discussed the effect of gradient hydrostatic pressure on the different mentioned parameters, namely, anisotropy factor, bulk modulus, shear modulus, Young's modulus, Lame's coefficient, Poisson's ratio, *B/G* ratio, calculated density, transverse, longitudinal and average sound velocity. Where, we have obtained a set of fitting coefficients of those parameters as functions of pressure.

Through quasi-harmonic approximation, we have studied also the temperature dependence of some thermodynamic functions and lattice heat capacity of both compounds for both types. We note that all calculated thermodynamic functions for both types for herein studied materials behave similarly under temperature gradient; the entropy increases, the free energy decreases algebraically and the internal energy increases with increasing temperature.

Both types of studied compounds have similar heat capacity variation *vs.* temperature. We note that in high temperature region C_v tends to the Petit and Dulong limit which is around 198 J/mol K for both types of the considered CZTX alloys.

Because of the similarity of the mechanical and thermodynamic properties of both considered types of the studied CZTX solar materials, the coexistence of both types does not influence the mechanical and thermodynamic behavior of the solar cells especially for the sulphide compound based solar cells compared to the selenide compound based solar cells.

We note that, to better design of CZTX samples for solar cells applications, elastic and thermodynamic data are important, therefore, our calculated results could be taken as a theoretical aided computer for CZTX material design for thin films based solar cells.

It is noted that, an analogue investigation for other solar materials is envisaged. As more attention is being paid to the application of these materials, it becomes necessary to have a complete and clear understanding of their physical properties in different structure configurations.

Appendix

APPENDIX

Density Functional Theory: Major Tool in Computational Materials Science

> *"A theory that gives such results must contains a great part of truth"*

A.1. Introduction

The study and understanding of natural systems is the main aim of physics theories. Since the structure on a microscale is responsible for the macroscale character of matter; the understanding and exploiting the properties of electrons and atomic-nuclei systems interacting is a primordial step in materials science. Through quantum theory, the fundamental properties of matter, and especially, in the condensed case are well known.

Full describing of atomic system requires the solving of *Schrödinger's* equation for the concerned system. Unfortunately, there are analytical solutions of this equation for very few simple systems, and accurate numerical solutions for just little number of atoms and molecules. However, in most cases, the use of approximations and assumptions is absolutely necessary.

The electrons and the nuclei constituting materials (atomic systems) are a strongly interacting system, this makes solving the *Schrödinger's* equation tremendously difficult. Quantum calculations are nowadays reliable and useful tools in the study of various properties of atomic systems (atoms, molecules, crystals…etc). There are mainly two types of quantum methods:

- Methods based on *Hartree-Fock* (HF) formalism, wherein the determination of the electronic properties of a molecular system with n electrons, requires knowledge of the polyelectronic wave function $\psi(1,2,...,n)$.
- Methods founded on Density Functional Theory (DFT), based on different approximations called *ab initio* methods or also *from first-principles* methods. With this theory, the properties of a many-electron system can be determined by using functionals, *i.e.* functions of another function, which in this case is the spatially dependent electron density.

Density Functional Theory is presently the most successful, and also the most promising approach to compute the electronic structure of matter. Its applicability ranges from atoms, molecules and solids to nuclei and quantum and classical fluids. It takes a primordial place in condensed-matter physics, computational physics, and computational chemistry. In its original formulation, the Density Functional Theory provides the ground state properties of a system, and the concept of electron density plays a key role.

In this appendix, we focus on the Density Functional Theory (henceforth DFT). Firstly, we give an overview of the famous Schrodinger equation. Then, we talk about derivation and formalism of DFT. In the end of this appendix, we explain the main features of used code to perform the calculations of our theoretical study *i.e.* CASTEP software program.

A.2. Schrodinger's equation

In 1926, the Austrian physicist *E. Schrödinger* published the first accounts of his now famous wave equation. Schrödinger's wave function seemed extremely promising, as it contains all of the information available about a system. The form of the Schrödinger equation depends on the physical situation. However, the most general form is the time-dependent Schrödinger equation, which gives a description of a system evolving with time (t) [1]:

$$i\hbar\frac{\partial}{\partial t}\Psi(\vec{r},t)=\hat{H}\Psi(\vec{r},t) \tag{A.1}$$

Here:

i : is the imaginary unit;

$\hbar$: is the reduced Planck constant or Dirac's constant ($\hbar=h/2\pi$; h: is the Planck's constant);

Ψ : is the wave function of the quantum system;

$\hat{H}$: is the Hamiltonian operator (which characterizes the total energy of any given wave function and takes different forms depending on the situation).

The time-independent Schrödinger equation predicts that wave functions can form stationary states also called "orbitals" (atomic orbitals or molecular orbitals). These states are important to solve the time-dependent Schrödinger equation. If the stationary states are well known, the solving of the time-dependent Schrödinger equation becomes fully accessible for any state. The stationary states satisfy the time-independent Schrödinger equation *i.e.*:

$$\hat{H}\psi(\vec{r})=E\psi(\vec{r}) \tag{A.2}$$

Here: $\hat{H}$: is the Hamiltonian operator;

ψ : is the wave function which represent a stationary state;

E: is the energy of the stationary state ψ.

For a solid system with *N* nuclei cores and *n* electrons, the Hamiltonian is written:

$$\hat{H} = -\sum_{i=1}^{n} \frac{\hbar^2}{2m} \vec{\nabla}_i^2 - \sum_{I=1}^{N} \frac{\hbar^2}{2M} \vec{\nabla}_I^2 - \sum_{i=1}^{n} \sum_{I=1}^{N} \frac{1}{4\pi\varepsilon_0} \frac{Z_I e^2}{\left|\vec{r}_i - \vec{R}_I\right|} + \sum_{i=1}^{n} \sum_{j>i}^{n} \frac{1}{4\pi\varepsilon_0} \frac{e^2}{\left|\vec{r}_i - \vec{r}_j\right|} + \sum_{I=1}^{N} \sum_{J>I}^{N} \frac{1}{4\pi\varepsilon_0} \frac{Z_I Z_J e^2}{\left|\vec{R}_I - \vec{R}_I\right|}$$

(A.3)

Here; m: is the mass of the electron;

$\left|\vec{r}_i - \vec{r}_j\right|$: is the distance between the electron *i* and the electron *j*;

M : is the mass of nucleus;

$\left|\vec{R}_I - \vec{R}_J\right|$: is the distance between the nucleus *I* and the nucleus *J*.

Z_I, Z_J : are the atomic numbers of the nuclei *I* and *J* respectively.

Under a reduced form; $\hat{H}$ is written as:

$$\hat{H} = \hat{T}_e + \hat{T}_N + \hat{V}_{eN} + \hat{V}_{ee} + \hat{V}_{NN} \qquad \text{(A.4)}$$

Here : $\hat{T}_e$: describes the kinetic energy of the electrons;

$\hat{T}_N$: describes the kinetic energy of the nuclei;

$\hat{V}_{eN}$: describes the electrons-nuclei interaction energy;

$\hat{V}_{ee}$: describes the electron-electron interaction energy;

$\hat{V}_{NN}$: describes the nucleus-nucleus interaction energy.

Practically, the most systems of interest consist of many interacting electrons, and the effort required to find solutions to the Schrödinger's equation increases enormously with the number of electrons. Unfortunately, in this form, Schrödinger's equation is excessively complex to be solved analytically.

As a result, we cannot obtain a general solution to this equation. Interestingly, this difficulty was recognized by Dirac as early as 1929, when he wrote "The underlying physical laws necessary for the mathematical theory of a large part of physics and the whole of chemistry are thus completely known, and the difficulty is only that the application of these laws leads to equations much too complicated to be soluble" [2]. Therefore, the use of approximations is indispensable.

A.3. Derivation and formalism

A.3.1. The Born-Oppenheimer approximation

In 1927, physicists *M. Born* and *J. R. Oppenheimer* [3] published an approximation method to simplify the resolution of *Schrödinger* equation and this in order to simplify the theoretical calculation of the energy levels and wave functions for molecules, which were before heavy stains to perform.

This approach called often the adiabatic approximation [3]. The *Born-Oppenheimer* approximation approach considers position of atomic nuclei as fixed; their kinetic energy can be neglected and the term of interaction between nuclei considered as a constant corresponds to the origin of energy. The equation to be solved is written then:

$$\hat{H}\psi = E\psi \Leftrightarrow \left[-\sum_{i=1}^{n} \frac{1}{2}\vec{\nabla}_i^2 - \sum_{i=1}^{n}\sum_{I=1}^{N} \frac{Z_I}{\left|\vec{r}_i - \vec{R}_I\right|} + \sum_{i=1}^{n}\sum_{j>i}^{n} \frac{1}{\left|\vec{r}_i - \vec{r}_j\right|} \right]\psi = E\psi \tag{A.5}$$

We note that, the employed units are the atomic units: unit of length is the Bohr (in a_0); $a_0 = 0.5292$ Å, $m_e=1$, $e=1$, $\hbar=1$ and $4\pi\varepsilon_0=1$. In the condensed form, equation (A.5) has the flowing expression:

$$\hat{H}\psi = E\psi \Leftrightarrow \left[\hat{T}_e + \hat{V}_{eN} + \hat{V}_{ee}\right]\psi = E\psi \tag{A.6}$$

Here; $\hat{H}$: called often the electronic Hamiltonian. By convention, the electron kinetic energy operator $\hat{T}_e$ is designated by T, the external potential felt by electrons (ionic potential) $\hat{V}_{eN}$ designated by V_{ext} and the potential of electron-electron interaction $\hat{V}_{ee}$ is designated by U. Therefore, the equation (A.6) is written as follows:

$$\left[T + V_{ext} + U\right]\psi = E\psi \tag{A.7}$$

Thus, the complexity of the problem is reduced to the behavior of electrons. However, the solving of the equation (A.7) is still difficult due to the interaction of a high number of electrons between themselves "*U*". Therefore, the development of other approximations is necessary to solve the problem.

Many methods have been developed to solve the multi-electronic *Schrödinger* equation (A.6). For example, in the *Hartree-Fock* method; the wave function is described as a *Slater* determinant. However, the problem with these methods is the huge computational effort, which makes it virtually impossible to apply them efficiently to larger, more complex systems. On the other hand, DFT provides an appealing alternative, being much more versatile as it provides a way to systematically map the many-body problem; considering the particle density as a basis quantity to describe a particular system.

A.3.2. The Hartree and Hartree-Fock approximation

Historically, the first attempt to give an approximate solution of the equation (A.2) is proposed by *Hartree* in 1928 [4]. The *Hartree* approximation consist to consider electrons as independent, each of them evolves in an average field created by all other electrons. This approximation reduces the problem of *n* electron in interaction onto single-electron system problem.

The Hamiltonian can be written as a sum of *n* Hamiltonians, each one, describes the behavior of a single electron:

$$H = \sum_{i=1}^{n} h_i \tag{A.8}$$

With the following expression for h_i:

$$h_i = -\frac{1}{2}\vec{\nabla}_i^2 + u_i\left(\vec{r}_i\right) + \mu_i\left(\vec{r}_i\right) \tag{A.9}$$

Here; the potential energy of the electron *i* in the field of all nuclei *I* ($u_i\left(\vec{r}_i\right)$) and the effective field of *Hartree* ($\mu_i\left(\vec{r}_i\right)$) have respectively the following expressions:

$$u_i\left(\vec{r}_i\right) = -\sum_I \frac{Z_I}{\left|\vec{r}_i - \vec{R}_I\right|} \tag{A.10}$$

$$\mu_i\left(\vec{r}_i\right) = \frac{1}{2}\sum_j \frac{1}{\left|\vec{r}_i - \vec{r}_j\right|} \tag{A.11}$$

The effective potential is the sum of these two contributions *i.e.*:

$$V_{eff}\left(\vec{r}\right) = \mu\left(\vec{r}\right) + u\left(\vec{r}\right) \tag{A.12}$$

By introducing the effective potential in the Schrödinger equation. We get:

$$\left[-\frac{1}{2}\vec{\nabla}_i^2 + V_{eff}\right]\psi_i\left(\vec{r}\right) = \varepsilon_i \psi_i\left(\vec{r}\right) \tag{A.13}$$

The wave function of the electronic system has a form of the product of wave functions of electrons, and the energy of the system equal to the sum of energies of all electrons.

$$\psi(\vec{r}_1,\vec{r}_2,...,\vec{r}_n)=\psi_1(\vec{r}_1)\psi_2(\vec{r}_2)...\psi_n(\vec{r}_n) \tag{A.14}$$

$$E = E_1 + E_2 + \ldots + E_n \tag{A.15}$$

The expression (A.14) is a solution of the equation (A.13). In 1930, *Fock* [5, 6] showed that *Hartree* wave function disobeys the exclusion principle of *Pauli*; because it is not anti-symmetrical with respect to the exchange of any two particles.

The approximation of *Hartree-Fock* [4-6] has been introduced to take into account the electron spin for solving *Schrödinger's* equation. The difference between the energy of the real multi-electronic system, and the energy obtained in the framework of *Hartree* approximation appears as the remaining electronic interactions. Allows the interactions that lacks in the *Hartree* approximation is the exchange-correlation.

The exchange has a purely quantum origin; it is the effect that expresses the anti-symmetry of the wave function with respect to the exchange of the coordinates of any two electrons, leading to describe the n-body (electron) system by the equality:

$$\psi(\vec{r}_1,\ldots,\vec{r}_a,\ldots,\vec{r}_b\ldots\vec{r}_n)=-\psi(\vec{r}_1,\ldots,\vec{r}_b,\ldots,\vec{r}_a\ldots\vec{r}_n) \tag{A.16}$$

Hartree, *Fock* and *Slater* [7] demonstrated that the anti-symmetric wave function of *Hartree* $\psi(\vec{r}_1,\vec{r}_2,...,\vec{r}_n)$ is written as a *Slater* determinant and checks the *Pauli* principle:

$$\psi(\vec{r}_1,\vec{r}_2,\ldots,\vec{r}_n)=\frac{1}{\sqrt{N!}}\begin{vmatrix}\psi_1(\vec{r}_1)\ldots\ldots\ldots\psi_1(\vec{r}_n)\\ \vdots\\ \vdots\\ \psi_n(\vec{r}_1)\ldots\ldots\ldots\psi_n(\vec{r}_n)\end{vmatrix} \tag{A.17}$$

This scheme gives good numerical results; however, the difference of energy between the correct and the *Hartree-Fock* fundamental energy can become very high if the distance between nuclei increases.

A.3.3. Density Functional Theory (DFT)

The purpose of the DFT, is to determine the properties of the ground state of a system consisting of fixed number of electrons in a Coulomb interaction with point nuclei, using only the electron density concept.

The predecessor to DFT was the *Thomas-Fermi* model developed in 1927 [8, 9], nevertheless, it could not have a theoretical justification than with the fundamental works of *Hohenberg* and *Kohn* in 1964 [10] and *Kohn* and *Sham* in 1965 [11] who proved the embodiment procedure of the DFT.

The fundamental concept of the density functional is that energy of an electronic system may be expressed as function of electron density $\rho(\vec{r})$, which minimizes the energy of the system.

The electron density $\rho(\vec{r})$ is a positive function, and has in particular, two important properties:

$$\begin{cases} \rho(\vec{r} \to \infty) = 0 \\ \int \rho(\vec{r})\, d\vec{r} = n \end{cases} \tag{A.18}$$

Therefore $\rho(\vec{r})$ represents by definition, the probability of finding an electron in a unit volume d^3r centered on the position $\vec{r}$. It seems to contain enough information to describe the system, while ψ has much more information, some of which are not necessary. Therefore, the electron density is sufficient to the complete determination of the properties for an atomic system.

A.3.3.1. Thomas-Fermi model

Both *Thomas* and *Fermi* developed the model independently in 1927 [8, 9]. They used a statistical model to approximate the distribution of electrons in an atom. The mathematical basis postulated that electrons are distributed uniformly in phase space with two electrons in every h^3 of volume. For each element of coordinate space volume, $d\vec{r}$ we can fill out a sphere of momentum space up to the *Fermi* momentum (p_F):

$$\frac{4}{3}\pi p_F^3(\vec{r}) \tag{A.19}$$

Equating the number of electrons in coordinate space to that in phase space gives:

$$\rho(\vec{r}) = \frac{8\pi}{3h^3} p_F^3(\vec{r}) \tag{A.20}$$

Solving this equation for p_F and substituting into the classical kinetic energy formula then leads directly to a kinetic energy represented as a functional of the electron density:

$$T_{TF}[\rho] = \frac{3}{10}\left(3\pi^2\right)^{2/3} \int \rho^{5/3}(\vec{r})\, d\vec{r} \tag{A.21}$$

In this way, it was possible to calculate the energy of an atom. Using this functional of kinetic energy combined with the classical expression of electron-nucleus and electron-electron interactions that can also be expressed in terms of electron density:

$$E_{TF}[\rho] = \frac{3}{10}\left(3\pi^2\right)^{2/3} \int \rho^{5/3}(\vec{r}) d\vec{r} + \int V_{ion}(\vec{r})\rho(\vec{r})\, d\vec{r} + \frac{1}{2}\int\int \frac{\rho(\vec{r})\rho(\vec{r}')}{|\vec{r}-\vec{r}'|} d\vec{r}d\vec{r}' \tag{A.22}$$

Although this was an important first step, the *Thomas-Fermi* equation accuracy is limited because the resulting kinetic energy functional is only approximate, and because the method does not attempt to represent the exchange energy of an atom as a conclusion of the *Pauli* principle.

Dirac added exchange energy functional in 1928. However, the *Thomas-Fermi-Dirac* theory remained rather inaccurate for most applications. The largest source of error was in the representation of the kinetic energy, followed by the errors in the exchange energy, and due to the complete neglect of electron correlation.

Teller (1962) showed that *Thomas-Fermi* theory cannot describe molecular bonding. This can be overcome by improving the kinetic energy functional by considering the *Weizsacker* correction:

$$T_W[\rho] = \frac{\hbar^2}{8m} \int \frac{|\nabla\rho(\vec{r})|^2}{\rho(\vec{r})} d\vec{r} \tag{A.23}$$

A.3.3.2. The theorems of Hohenberg and Kohn

The development of the DFT began in the years 1964 and 1965 with the famous contribution of *P. Hohenberg* and *W. Kohn* (1964) [10]. Both authors have demonstrated two fundamental theorems whose statements are:

First Theorem: *The total energy E of the ground state is a unique functional of the particle density* $\rho(\vec{r})$ *for a given external potential* $v_{ext}(\vec{r})$.

This theorem means that it is sufficient to know only the electron density to determine all wave functions. Accordingly, the total energy E of an interacting electrons system in an external potential is represented as a functional of the electron density of the ground state ($\rho_0(\vec{r})$) in the flowing manner:

$$\begin{aligned} E &= \langle\psi|\hat{H}|\psi\rangle = \langle\psi|\hat{T}+\hat{U}+\hat{V}|\psi\rangle = \langle\psi|\hat{T}+\hat{U}|\psi\rangle + \int V_{ext}(\vec{r})\rho(\vec{r})\,d^3r \\ &= F[\rho]+V[\rho] = T[\rho]+U[\rho]+V[\rho] \end{aligned} \tag{A.24}$$

$$\begin{aligned} F[\rho] &= \langle\psi|\hat{T}+\hat{U}|\psi\rangle \\ V[\rho] &= \int V_{ext}(\vec{r})\rho(\vec{r})\,d^3r \end{aligned} \tag{A.25}$$

T and U are the kinetic energy and the inter-particle interaction potential respectively that do not depend on the external potential $V_{ext}(\vec{r})$. Thus, $F[\rho]$ is a universal functional of $\rho(\vec{r})$ which contains kinetic and Coulomb contributions to the energy, while V is called a non-universal functional, as it depends on the studied system.

Second Theorem: (Variational principle); the functional of the total energy for all system of many particles possesses a minimum which corresponds to the ground stat. The particle density of the ground state checks: $E(\rho_0) = \min E(\rho)$.

Hohenberg and *Kohn* demonstrated that the exact density of the ground state is the one that minimizes the energy $E(\rho)$ according to the variational principle; furthermore, all other properties are a functional of this particle density.

A.3.3.3. The Kohn-Sham approach or Kohn's and Sham's Ansatz

"If you don't like the answer, change the question"

After several years of efforts, *W. Kohn* and *L. J. Sham* (1965) [11] imposed their approach that consist to replace the interacting system with an equivalent isolated system, brought to the same density as that of the real system, in which, a base of n orbitals is used. Therefore, the imposed approach leaves undetermined the smallest term of the total energy *i.e.* the exchange-correlation term.

This approach is intended to determine the electronic-wave functions that minimize the total energy of the system. The wave functions are determined from a similar equation to the *Schrödinger* equation with a self-consistent (*i.e.* iterative) manner given by [11]:

$$\left[-\frac{1}{2}\vec{\nabla}^2 + V_{ext}(\vec{r}) + V_H(\vec{r}) + V_{XC}(\vec{r})\right]\psi_i(\vec{r}) = \varepsilon_i\psi_i(\vec{r}) \tag{A.26}$$

$\psi_i(\vec{r})$: is the wave function of the i^{th} electron;

$V_{ext}(\vec{r})$: is the external -ionic- potential;

$V_H(\vec{r})$: is the term of *Hartree* given by:

$$V_H(\vec{r}) = \int\int \frac{\rho(\vec{r}_1)\rho(\vec{r}_2)}{|\vec{r}_1 - \vec{r}_2|} d\vec{r}_1 d\vec{r}_2 \tag{A.27}$$

V_{xc} : is the exchange correlation potential

The fictitious electron system without interaction immersed in an effective potential V_{eff} which is that of the real system:

$$V_{eff} = V_H + V_{XC} + V_{ext} \tag{A.28}$$

Here:

V_H : is the *Hartree* potential given by:

$$V_H = \int \frac{\rho(\vec{r}\,')}{|\vec{r} - \vec{r}\,'|} d\vec{r}\,' \tag{A.29}$$

V_{ext} : is the external -ionic- potential;

V_{XC} : is the exchange correlation potential that is given by:

$$V_{XC} = V_C + V_X \tag{A.30}$$

The potential of exchange-correlation is obtained from the derivative of the exchange-correlation energy E_{XC} with respect to the density:

$$V_{XC}(\vec{r}) = \frac{\partial E_{XC}\left[\rho(\vec{r})\right]}{\partial \rho(\vec{r})} \tag{A.31}$$

Consequently, the equations of Kohn-Sham (K-S) can be written as:

$$H\psi_i(\vec{r}) = \left[-\frac{1}{2}\vec{\nabla}^2 + V_{eff}(\vec{r})\right]\psi_i(\vec{r}) = \varepsilon_i \psi_i(\vec{r}) \tag{A.32}$$

This eigenvalue equation is the typical representation of the *Kohn-Sham* equations. Here, ε_i is the orbital energy of the corresponding *Kohn-Sham* orbital ψ_i and the electron density for an *n* electron system is:

$$\rho(\vec{r}) = \sum_{i=1}^{n} |\psi_i(\vec{r})|^2 \tag{A.33}$$

The orbitals of K-S are described by the following expression:

$$\psi_i\left(\vec{k},\vec{r}\right)=\sum_j C_{ij}\phi_j\left(\vec{k},\vec{r}\right) \tag{A.34}$$

$\phi_j\left(\vec{k},\vec{r}\right)$: represent the functions of the base.

C_{ij} : are the expansion coefficients.

The solutions of K-S equations return to determine the C_{ij} coefficients for occupied orbitals that minimize the total energy. If the bases are given, the Hamiltonian and overlap matrixes, H and S respectively, are constructed. The secular equation is defined as follows:

$$\left(H-\phi\varepsilon_i S\right)C_i=0 \tag{A.35}$$

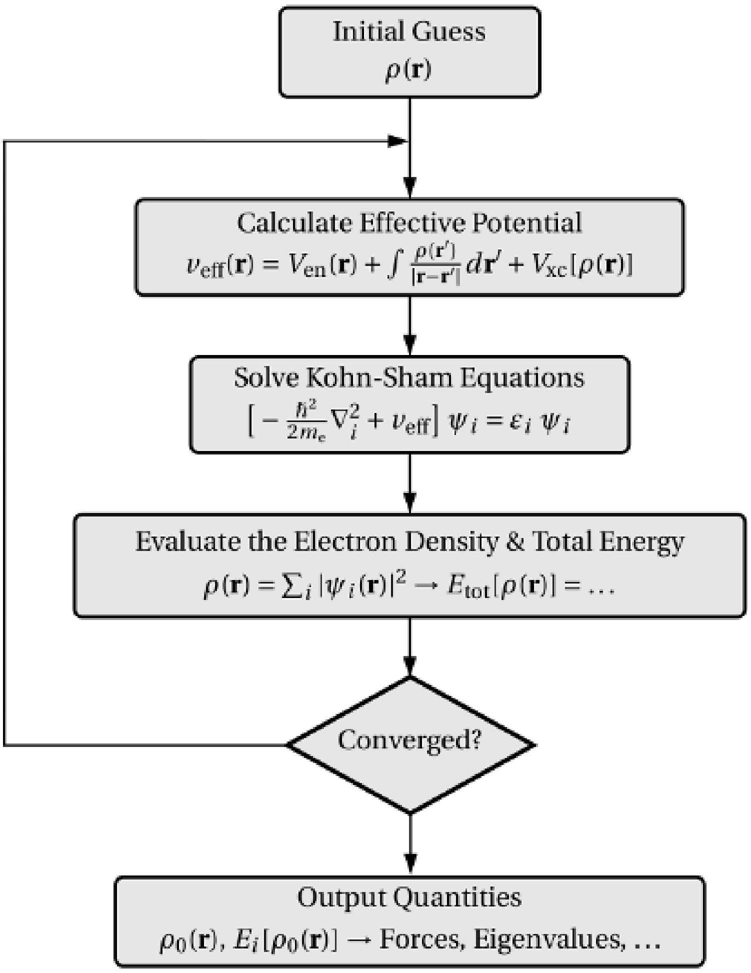

Fig.A.1: *Schematic representation of the organization chart of K-S equations resolution within self-consistent (i.e., iterative) way based on an initial guess and convergence criteria* [12].

By virtue of the accuracy of the K-S scheme, as well as the exact knowledge of the functional $E_{XC}(\rho)$; thus, we could envisage an exact description of all physical effects of electronic interaction, obviously including the effects of correlation. However, the use of DFT and the Kohn-Sham equations in practice requires the introduction formulation for $E_{XC}\left[\rho(\vec{r})\right]$, for this purpose, several approximations have been proposed.

A.3.3.4. Approximations based on DFT

To approximate the exchange-correlation functional $E_{XC}\left[\rho(\vec{r})\right]$; three types of functional are available: local (LDA), gradient-corrected (GGA) and fully nonlocal (based on the exact and screened exchange formalism). We talk about the main proposed functional, that are the Local Density Approximation (LDA) and the Generalized Gradient Approximation (GGA).

A.3.3.4.1. Local Density Approximation (LDA)

To approximate the density functional $E_{XC}\left[\rho(\vec{r})\right]$, *Kohn* and *Sham* proposed in 1965 the Local Density Approximation (LDA). In this approximation, it is assumed that, the electron density varies sufficiently slowly in the system, so that we can write:

$$E_{XC}^{LDA}\left[\rho(\vec{r})\right]=\int \rho(\vec{r})\varepsilon_{XC}^{LDA}\left[\rho(\vec{r})\right]d\vec{r} \tag{A.36}$$

Where $\varepsilon_{XC}^{LDA}\left[\rho(\vec{r})\right]$: is the energy density of a homogeneous electron gas of density $\rho(\vec{r})$. In other words, it is assumed that around each point $\vec{r}$ the real system can be replaced by a homogeneous electron gas of density $\rho(\vec{r})$.

We note that, there are many works that focus on the parameterization of $\varepsilon_{XC}^{LDA}\left[\rho(\vec{r})\right]$; such as those of *Vosko, Wilk* and *Nusair* [13], and *Perdew* and *Zunger* [14]. It is noted that, all these functionals generally lead to very similar results.

A.3.3.4.2. Generalized Gradient Approximation (GGA)

The obtained results from LDA-based calculations are often satisfactory. Nevertheless, the Generalized Gradient Approximation (GGA) may improve the obtained results compared to experimental ones. It takes into account the local variations of the electron density through its gradient $\vec{\nabla}\rho(\vec{r})$; consequently it provides a significant increase in the accuracy of the calculated results.

In the framework of the Generalized Gradient Approximation (GGA), the energy of exchange-correlation E_{XC} is a function of the electron density $\rho(\vec{r})$ and its gradient $\vec{\nabla}\rho(\vec{r})$:

$$E_{XC}^{GGA}\left[\rho(\vec{r})\right]=\int f\left\{\rho(\vec{r}),\vec{\nabla}\rho(\vec{r})\right\}d\vec{r} \qquad \text{(A.37)}$$

Here, f is a function of the local density and its gradient. It is noted that, several parameterizations of this function have been proposed, the most used is that proposed by *Perdew-Burke* and *Enzerhoft* [15] in 1996.

A.4. Plane Wave Pseudo-Potential method (PW-PP)

Efficiency of the calculations based on DFT is due essentially to the efficiency of Pseudo-Potential Plane Wave method (PP-PW). We explain in this section, the theorem of Bloch and the pseudo-potential approach.

A.4.1. Bloch's theorem

Bloch's theorem states that in a periodic solid; the electronic wave function can be written as the product of a cell-periodic part and a wave plane part [16].

$$\begin{aligned}\psi_i(\vec{r}) &= f_i(\vec{r})\exp\left[i\vec{k}.\vec{r}\right]\\ f_i(\vec{r}) &= f_i\left(\vec{r}+\vec{R}\right)\end{aligned} \qquad \text{(A.38)}$$

Here $\vec{k}$ is a vector of reciprocal space confined in the first *Brillouin* zone, *i* is the band index and $\vec{R}$ vector of direct lattice *i.e. Bravais* lattice. The cell-periodic part of the wave function can be expanded using a basis set consisting of a discrete set of plane waves whose wave vectors are reciprocal lattice vectors of the crystal:

$$f_i(\vec{r})=\sum_G c_{i,G}\exp\left[i\vec{G}.\vec{r}\right] \qquad \text{(A.39)}$$

Where, the reciprocal lattice vectors $\vec{G}$ are defined by; $\vec{G}.\vec{R}=2\pi m$, for all $\vec{R}$; where $\vec{R}$ is a lattice vector of the crystal and m is an integer. Therefore, each electronic function can be written as a sum of plane waves:

$$\psi_i(\vec{r}) = \sum_G c_{i,k+G} \exp\left[i\left(\vec{k}+\vec{G}\right).\vec{r}\right] \tag{A.40}$$

Bearing in mind that, the 1st *Brillouin* zone contains an infinite number of $\vec{k}$ points that requires an infinite plane waves basis set to rebuild completely the system by symmetry. To overcome this problem, the calculation is performed by sampling the first Brillouin zone into specific sets of $\vec{k}$ points.

In this purpose, various sampling methods of the first *Brillouin* zone have been proposed to perform calculations, such as, the method of *Shadi* and *Cohn* [17], *Evarestove* and *Smirnov* [18], *Joannopoulos* and *Cohn* [19], and *Monkhorst* and *Pack* [20].

A.4.2. Pseudo-potential approach

Let us consider a solid as a collection of valence electrons and ion cores. The ion cores contain nuclei and strongly bound core electrons. In the pseudo-potential approach ion cores are considered to be frozen. This means that properties of molecules or solids are calculated on the assumption that the ion cores are not involved in chemical bonding and consequently, they are little affected under foreign changes.

In this approach the all electron strong Coulomb potential Z/r is replaced by a weaker pseudo-potential V_{pseudo}. However, the wave functions $\psi(\vec{r})$ representing the valence electrons are replaced by pseudo-wave functions $\psi^{ps}(\vec{r})$; see Fig.A.2. The equality $\psi_{pseudo}(\vec{r}) = \psi(\vec{r})$ is imposed on the outside of a sphere with radius r_c around the atom, in the inside of this sphere; the $\psi_{pseudo}(\vec{r})$ form is chosen to remove knots and oscillations due to the orthogonality of the wave functions [21].

These pseudo-wave functions have the advantage of being represented in the Fourier space by a very reduced number of plane waves, and this reduces significantly the numerical calculations. We note that, the potential undergoes also a similar treatment. The pseudo-potential form is chosen in the manner that the pseudo-wave functions and the valence of wave functions have the same proper energies [22].

There are three types of pseudo-potential, each of them has their advantages and disadvantages:

- Norm-conserving pseudo-potentials introduced by Humman et al [23-26];
- Dual-space Gaussian pseudo-potentials introduced by Goedecker et al [27];

- Ultra-soft pseudo-potentials introduced by Vanderbilt [28].

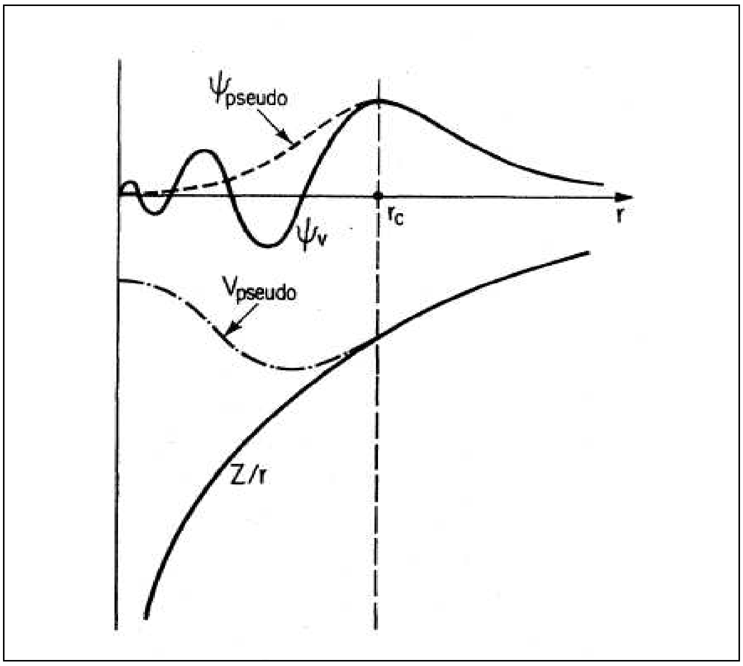

Fig.A.2: *Schematic illustration of all-electron (solid lines) and pseudoelectron (dashed lines) potentials and their corresponding wave functions. The radius at which all-electron and pseudoelectron values match is designated* r_c [21].

The use of pseudo-potential in the formalism of DFT has proved a considerable success in recent years, in calculations and predictions of the properties of the ground state of solid materials. It is noted that, the primordial aim of the pseudo-potential employment is the huge reduction of the expense of the calculations; because in this approach the performed calculations deal explicitly only with valence electrons. In the following section, we talk about the most popular used pseudo-potentials in the framework of DFT-based calculations *i.e.* Norm-conserving pseudo-potentials and Ultra soft pseudo-potentials.

A.4.2.1. Norm-conserving pseudo-potentials (NCP)

A valid pseudo-potential should be soft and transferable. The term "soft" is used to describe a pseudo-potential that requires little plane waves to represent the pseudo wave function. Concerning the transferability, which means that, the generated pseudo-potential for a given atomic configuration must reproduce exactly the other configurations. For this, the concept of the conservation of the norm is employed. In this category of pseudo-potentials, the pseudo wave functions are constructed to be equal to the real wave functions in the outside of a core within a radius of r_c.

A.4.2.2. Ultra soft pseudo-potentials (USP)

Ultra soft pseudo-potentials (USP) were introduced by Vanderbilt in (1990) [28] in order to allow calculations to be performed with the lowest possible cut-off energy for the plane-wave basis set. This new class of pseudo-potentials is characterized by pseudo-wave functions, which can be arbitrarily smoothed in the core region. In this approach, high values of r_c can then be used, and therefore, the cut-off energy of the plane wave necessary for the calculations can be considerably reduced.

A.5. Choice of the basis set projection for the electronic wave functions

There are several bases that serve to expand the electronic wave functions at each k-point, such as: Planes Waves (PW), Orthogonalized Planes Waves (OPW), Augmented Planes Waves (APW) and that of Linearized Augmented Planes Waves (LAPW).

The used code in our work "CASTEP" exploits the Planes Waves as a basis set that satisfy the Bloch's theorem. Therefore, the decomposition of the wave functions into plane waves consists to express the electronic wave functions through Fourier series as follows:

$$\psi_n\left(\vec{k},n\right)=\sum_G G_n\left(k,G\right)\exp\left[i\left(\vec{k}+\vec{G}\right).\vec{r}\right] \tag{A.41}$$

In principle, an infinite number of plane waves, is required for such an expansion, which is not the case in practice. Thus, the plane wave basis set can be truncated by limiting the set of plane waves taken into consideration by introducing a cut-off energy $E_{cut-off}$ defined by:

$$E_{cut-off} \geq \frac{\hbar^2}{2m}\left|\vec{k}+\vec{G}\right|^2 \tag{A.42}$$

If this energy is too low, the number of plane waves in the calculation is not enough to represent properly the wave functions of the charge density functions, so we must appropriately choose this energy.

A.6. About using CASTEP code in our calculations

The abbreviation stands for Cambridge Serial Total Energy Package; CASTEP is a state of the art quantum mechanics-based software program, it is designed for materials science and especially condensed-matter discipline [29]. CASTEP employs the Density Functional Theory Plane-Wave Pseudo-Potential method (PW-PP), which allows us to perform first-principles quantum mechanics calculations in order to explore the properties of crystals and surfaces in substances such as semiconductors, ceramics and metals. The CASTEP code can currently perform five different tasks [29]:

- Single-point energy calculation
- Geometry optimization
- Molecular dynamics
- Elastic constants calculation
- Transition-state search
- Properties

The CASTEP "Properties" task allows us to compute numerous properties, namely; electronic, structural, and vibrational properties after the achievement of single-point energy, geometry optimization, or dynamics run on a 3D periodic system. We summarize the main properties that can be calculated using CASTEP code [29]:

- Band structure: calculation of the electronic eigenvalues along high-symmetry directions in the Brillouin zone. Either, the value of band gap is provided through band-structure calculations.
- Core level spectroscopy: this property enables to calculate the electronic energies on the Monkhorst-Pack mesh of k-points and the matrix elements for electronic inter-band transitions.
- Density of states: selecting this property, electronic eigenvalues on a fine Monkhorst-Pack grid are calculated non-self-consistently considering both valence and conduction bands, by means of electronic charge densities and potentials generated during the simulation.
- Electron density difference: allows us to compute the electron density difference with respect to either a linear combination of the atomic densities or a linear combination of the densities of sets of atoms contained in the studied structure.
- Electron localization function: this property provides a simple measure of electron localization in atomic and molecular systems.
- Optical properties: Matrix elements for electronic inter-band transitions are computed.
- Orbitals: Information about electronic-wave functions is given.

- Phonons: For phonon dispersion calculations, phonon frequencies and eigenvectors along high symmetry directions in the Brillouin zone are considered. However, in the case of phonon density of states calculations, phonon frequencies and eigenvectors are provided on a Monkhorst-Pack grid. This task is used to calculate thermodynamic properties.
- Population analysis: in the framework of this property, both Mulliken analysis and Hirshfeld charge analysis may be performed.

References

[1] R. Shankar, *Principles of Quantum Mechanics*, 2nd edition, Kluwer Academic Plenum Publishers, New York, 1994.

[2] P. A. M. Dirac. *Quantum mechanics of many-electron systems*. Proceedings of the Royal Society of London. Series A, Containing Papers of a Mathematical and Physical Character, 123 (792) 714 1929.

[3] M. Born, J. R. Oppenheimer, Ann. Phys. 87 (1927) 457.

[4] D. R. Hartree, Proc. Cambridge Philos. Soc. 24 (1928) 89.

[5] V. Fock, Z. Phys. 61 (1930) 126.

[6] V. Fock, Z. Phys. 62 (1930) 795.

[7] J. C. Slater, Phys. Rev. 35 (1930) 210.

[8] L .H. Thomas, Pro. Cambridge Philos. Soc. 23 (1927) 542.

[9] E. Fermi, Z. Phys. 48 (1928) 73.

[10] P. Hohenberg, W. Kohn, Phys. Rev. B 136 (1964) 864.

[11] W. Kohn, L. J. Sham, Phys. Rev. A 1133 (1965) 140.

[12] W. Gös, *Hole Trapping and the Negative Bias Temperature Instability*, Ph.D. Dissertation Fakultät für Elektrotechnik und Informationstechnik, Technischen Universität Wien, Wien, 2011.

[13] J. P. Zunger, A. Perdew, Phys. Rev. B 23 (1981) 5048.

[14] S. H. Vosko, L. Wilk, M. Nusair, Can. J. Phys. 58 (1980) 1200.

[15] J. P. Perdew, K. Burke, M. Ernzerhof, Phys. Rev. Lett. 77 (1996) 3865.

[16] N. W. Ashcroft, N. D. Mermin, Solid State Physics, Harcourt, Florida, 1976.

[17] D. J. Shadi, M. L. Cohn. Phys. Rev. B 8 (1973) 5747.

[18] R. A. Evarestov, V. P. Smirnov, Phys. Status Solidi, 9 (1983) 119.

[19] J. D. Joannopoulos, M. L. Cohn, J. Phys. C 6 (1973) 1572.

[20] H. J. Monkhorst, J. D. Pack, Phys. Rev. B 13 (1976) 5188.

[21] M. C. Payne, M. P. Teter, D. C. Allan, T. A. Arias, J. D. Joannopoulos. Rev. Mod. Phys. 64 (1992) 1045.

[22] W. E. Pikett, Computer Physics Report, 9 (1989) 115.

[23] D. R. Hamman, M. Schluter, C. Chiang, Phys. Rev. Lett. 43 (1981) 1494.

[24] N. Troullier, J. L. Martins, Phys. Rev. B 43 (1991) 1993.

[25] C. Hartwigsen, S. Goedecker, J. Hutter, Phys. Rev. B 58 (1998) 3641.

[26] G. B. Bachelet, D. R. Hamann, M. Schlüter, Phys. Rev. B 26 (1982) 4199.

[27] S. Goedecker, M. Teter, J. Hutter. Phys. Rev. B 54 (1996) 1703.

[28] D. Vanderbilt, Phys. Rev. B 41 (1990) 7892.

[29] Materials Studio CASTEP Online Help: http://www.tcm.phy.cam.ac.uk/castep/documentation/WebHelp/CASTEP.html (Jun, 10th 2014).

ABSTRACT

In this thesis, we have studied some physical properties of Copper-Zinc-Tin-(Sulphide, Selenide) or Cu_2ZnSnX_4 (X=S and Se) solar materials for the kesterite (KS) and stannite (ST) types by employing first principles calculation approach, using the plane wave pseudo potential calculations (PP-PW) implemented in the CASTEP package within Density Functional Theory (DFT) and the Generalized Gradient Approximation of Wu-Cohen (GGA-WC). The calculated lattice parameters are in good agreement with experimental reported data. The elastic constants are calculated for both types of both compounds using the static finite strain scheme; the pressure dependence of elastic constants is predicted. The bulk modulus, anisotropy factor, shear modulus, Young's modulus, Lame's coefficient and Poisson's ratio have been estimated from the calculated single crystalline elastic constants. The analysis of *B/G* ratio shows that these compounds behave as ductile. Through quasi-harmonic approximation, the temperature dependence of some thermodynamic functions and lattice heat capacity of both compounds for both types have been performed.

Key words: CZTS, CZTSe, First principles, Elastic constants, Thermodynamic properties.

RÉSUMÉ

Dans cette thèse, nous avons étudié certaines propriétés physiques de matériaux solaires Cuivre-Zinc-Etain-(Soufre, Selenium) ou Cu_2ZnSnX_4 (X=S et Se) pour les deux types de structure kesterite (KS) et stannite (ST) par l'approche de calcul de premiers principes, en utilisant la méthode de calcul des ondes planes pseudo potentiel (PP-PW) implémentée dans le code CASTEP qui se base sur la théorie de la fonctionnelle de la densité (DFT), et l’approximation généralisée de gradient de Wu-Cohen (GGA-WC). Les paramètres de maille calculés sont en bon accord avec les données expérimentales disponibles. Les constantes élastiques sont calculées pour les deux types de composés en utilisant la technique des déformations finies statiques; la dépendance en pression hydrostatique des constantes élastiques est aussi prédite. Le module de compressibilité, le facteur d'anisotropie, le module de cisaillement, le module de Young, le coefficient de Lamé et le rapport de Poisson ont été estimés à partir des constantes élastiques calculées du monocristal. L'analyse du rapport *B/G* montre que les composés CZTX se comportent comme ductile. En employant l'approximation quasi-harmonique, la dépendance en température de certaines fonctions thermodynamiques et la capacité calorifique de deux composés pour les deux types ont été effectués.

Mots clés: CZTS, CZTSe, Premiers principes, Constantes élastiques, Propriétés thermodynamiques.

ملخص

في هذه الأطروحة، تمت دارسة بعض الخواص الفيزيائية للمركبات الشمسية نحاس-زنك-قصدير- (كبريت، سيلينيوم) أو Cu_2ZnSnX_4 (X = S, Se) لكلا النوعين kesterite (KS) وstannite (ST) عن طريق مقاربة حسابية من المبادئ الأولى، باستخدام طريقة الموجة المستوية والكمون الزائف (PP-PW) المدخلة في البرنامج CASTEP الذي يقوم على نظرية دالية الكثافة (DFT)، و تقريب التدرج المعمم (GGA-WC). المعاملات البنيوية المحسوبة في اتفاق جيد مع البيانات التجريبية المتوفرة. حساب ثوابت المرونة لكلا النوعين للمركبين المدروسين تم باستخدام تقنية التشوهات المحدودة الساكنة؛ تم أيضا التنبؤ بسلوك ثوابت المرونة بدلالة الضغط الهيدروستتيكي. معامل الانضغاط، عامل التباين، معامل القص، معامل يونغ، معامل لامي ومعامل بواسون قدرت من الثوابت المرنة للبلور الأحادي. تحليل النسبة *B/G* تبين أن المركبات CZTX لها تصرف ميكانيكي لين. باستخدام تقريب شبه التوافقي، تمت دراسة التعلق بدرجة الحرارة لبعض الدوال الترموديناميكية والسعة الحرارية لكلا النوعين للمركبين المدروسين.

كلمات مفتاحية : CZTSe, CZTS ، المبادئ الأولى، ثوابت المرونة، الخصائص الترموديناميكية.